E6-2025-57

I. N. Izosimov [1,*]

STRUCTURE OF THE β-DECAY STRENGTH FUNCTION

Submitted to "Chinese Physics C"

[1] Joint Institute for Nuclear Research, 141980, Dubna, Russia
[*] E-mail: izosimov@jinr.ru

Изосимов И. Н. E6-2025-57

Структура силовой функции β-распада

Проанализированы экспериментальные данные измерений резонансной и тонкой структуры силовой функции бета-распада $S_\beta(E)$ в сферических, переходных, деформированных и гало-ядрах. Современные методы ядерной спектроскопии позволили выявить расщепление пиков в $S_\beta(E)$, вызванное деформацией ядра, для переходов типа Гамова–Теллера (ГТ). Экспериментально доказана резонансная структура $S_\beta(E)$ для переходов первого порядка запрета (FF) как в сферических, так и в деформированных ядрах. Показано, что при некоторых энергиях возбуждения ядер FF-переходы могут быть сравнимы по интенсивности с ГТ-переходами. Проведен анализ разности энергий ГТ-резонанса (ГТР) и изобар-аналогового резонанса (ИАР) ($E_{\text{ГТР}}-E_{\text{ИАР}}$) при увеличении нейтронного избытка в ядре. Предсказана область спин-изоспиновой $SU(4)$ симметрии Вигнера.

Работа выполнена в Лаборатории ядерных реакций им. Г. Н. Флерова ОИЯИ.

Препринт Объединенного института ядерных исследований. Дубна, 2025

Izosimov I. N. E6-2025-57

Structure of the β-Decay Strength Function

The experimental measurement data on the resonance and fine structure of the beta-decay strength function $S_\beta(E)$ in spherical, transitional, deformed and halo nuclei are analyzed. Modern nuclear spectroscopy methods allowed the split of the peaks caused by nuclear deformation to be revealed in $S_\beta(E)$ for transitions of the Gamow–Teller (GT) type. The resonance structure of $S_\beta(E)$ for first-forbidden (FF) transitions in both spherical and deformed nuclei is experimentally proved. It is shown that at some nuclear excitation energies, FF transitions can be comparable in intensity with GT transitions. Analysis of the evolution of the energy differences ($E_{\text{GTR}}-E_{\text{IAR}}$) between the GT resonance (GTR) and the isobar-analog resonance (IAR) with an increase of the neutron excess in the nuclei was done. The $SU(4)$ Wigner's spin–isospin symmetry region was predicted.

The investigation has been performed at the Flerov Laboratory of Nuclear Reactions, JINR.

Preprint of the Joint Institute for Nuclear Research. Dubna, 2025

INTRODUCTION

The strength function for β transitions $S_\beta(E)$ is one of the most important characteristics of an atomic nucleus [1–6]. It is a distribution of moduli squared of β-decay type matrix elements in nuclear excitation energies E. At energies E up to Q_β (total β-decay energy), $S_\beta(E)$ defines the character of the β decay and the half-life $T_{1/2}$ of a radioactive nucleus against the β decay. At high energies unachievable in the β decay, $S_\beta(E)$ defines cross sections for various nuclear reactions that depend on the β-decay type matrix elements.

The β-decay probability is proportional to a product of the lepton part described by the Fermi function $f(Q_\beta - E)$ and the nucleon part described by $S_\beta(E)$. Since the Fermi function rapidly decreases (Fig. 1) with increasing E, the probability of β transitions at excitation energies E larger than 3–4 MeV in medium and heavy nuclei can be small. However, from the point of view of the nuclear structure and description of the β decay, it is the character of $S_\beta(E)$ at excitation energies larger than 3–4 MeV that is most interesting. When $E > 3{-}4$ MeV, resonances caused by the nuclear structure and residual spin–isospin interaction arise in $S_\beta(E)$ [1–6].

By measuring populations of levels in the β decay, one can find [4, 6, 7] the reduced probabilities $(1/ft)$ and the strength function $(S_\beta(E) \sim 1/ft(E))$ for the β decay. Until recently, the $S_\beta(E)$ structure was experimentally studied by using total absorption gamma-ray spectrometers and total absorption

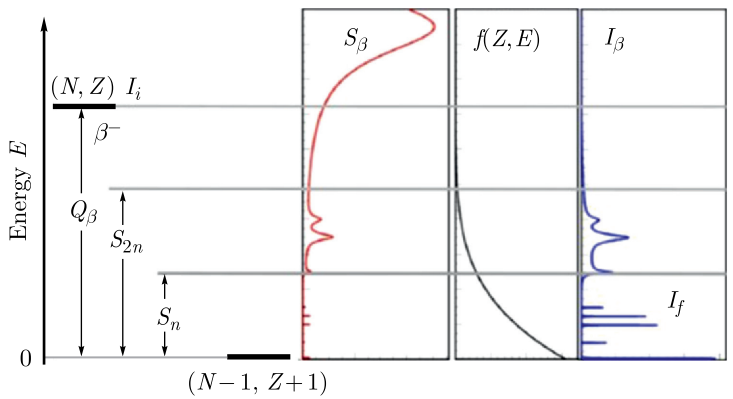

Fig. 1. Diagram of the β decay and its components. S_β is the β-decay strength function, $f(Z,E)$ — Fermi function, I_β is level population after the β decay, S_{xn} is the separation energy of x neutrons, I_i and I_f are the spins of initial and final states

spectroscopy (TAS) methods [4, 6–11], where γ rays accompanying the β decay were detected by large NaI crystals in the 4π geometry. If the total absorption efficiency for γ rays is large enough, total absorption peaks, whose intensity is governed solely by the probability of β-decay population of levels, can be identified in the spectra. This method allowed the resonant structure of $S_\beta(E)$ for Gamow–Teller (GT) β transitions to be experimentally demonstrated [4, 6, 7]. However, TAS methods have some disadvantages arising from a low energy resolution of NaI-based spectrometers. Only one or two total absorption peaks can be identified in TAS spectra, isobaric impurities in the analyzed source often give rise to uncertainties, Gamow–Teller and first-forbidden (FF) β transitions cannot be separated, the fine structure of $S_\beta(E)$ cannot be measured, and problems often arise in processing the spectra. Therefore, it appears important to measure $S_\beta(E)$ by using methods of high-resolution γ spectroscopy. Development of experimental techniques allows application of methods of nuclear spectroscopy with high energy resolution for the $S_\beta(E)$ fine structure measurement [7, 11–15]. Only in the past years, with great advances in production of monoisotopic radioactive sources and the advent of semiconductor HPGe γ-ray detectors combining high energy resolution and adequate efficiency, has it become possible to measure $S_\beta(E)$ with high confidence and high energy resolution. This allows thorough investigation of $S_\beta(E)$ at a qualitatively new level [11–15]. It was shown that the high-resolution nuclear spectroscopy methods give conclusive evidence of the $S_\beta(E)$ resonance structure both for GT and FF β decays in deformed, spherical and transitional nuclei. The combination of TAS with high-resolution γ spectroscopy may be applied for detailed decay schemes construction [11, 15]. It was experimentally shown that for some excitation energies of daughter nuclei, the probability of FF β^+/EC transitions is comparable with that of GT β^+/EC transitions. High-resolution nuclear spectroscopy methods [11–14] made it possible for the first time to demonstrate experimentally the resonance nature of $S_\beta(E)$ for FF β transitions and reveal splitting of the peak in $S_\beta(E)$ for the GT β decay of the deformed nuclei into two components. This splitting indicates anisotropy of oscillation of the isovector nuclear density component.

The structure of $S_\beta(E)$ for halo nuclei was analyzed in [16–21]. The Gamow–Teller resonance (GTR) and resonances in GT β-decay strength function $S_\beta(E)$ for halo nuclei may have the structure corresponding to *np* tango halo [18, 20]. When neutron excess is high enough, resonances in $S_\beta(E)$ may simultaneously have both nn Borromean halo component and np tango halo component and form the so-called mixed halo.

One of the consequences of the Wigner [21, 22] spin–isospin $SU(4)$ symmetry is $E_{\mathrm{GTR}} = E_{\mathrm{IAR}}$, where E_{GTR} is the energy of the GT resonance and E_{IAR} is the energy of the isobar-analog resonance (IAR). $SU(4)$ symmetry-restoration effect is induced by the residual interaction, which displaces the GT resonance towards IAR with increasing $(N - Z)/A$. Study of $S_\beta(E)$ for halo nuclei allows demonstrating that the value $Z/N \approx 0.6$ may correspond to the $SU(4)$ symmetry region [21, 22].

The theory of GT- and FF-type excitations is in a stage of development, one can therefore hope for qualitatively new facts and ideas about nuclear structure, as usually happens when new phenomena and new regions of nuclei are investigated.

1. RESONANCE STRUCTURE OF THE β-DECAY STRENGTH FUNCTIONS

The β decay of atomic nuclei is a charge-exchange process where nuclear states with a large fraction of charge-exchange configurations are populated with the highest intensity. The wavelengths of leptons emitted in the β decay of atomic nuclei are usually large compared to the size of the nucleus; therefore, the β-transition amplitude can be considered, in a number of cases, independent of the position and velocity of nucleons [23, 24]. The parity of nuclear states does not change in allowed transitions. Transitions able to be considered in this approximation are called "allowed transitions". Allowed β transitions can be divided into two types, namely, Fermi (F) and Gamow–Teller (GT). For Fermi-type transitions, the transition operator does not depend on the nucleon spin, and for Gamow–Teller-type transitions, it is proportional to the spin operator of the decaying nucleon. The Fermi-type transition operator is a component of the total isospin, and the transition matrix element depends only on the isospin quantum numbers of the initial and final nuclear states. In Fermi-type transitions, there is no angular momentum exchange between nucleons and leptons, whereas in GT transitions, a unit angular momentum is transferred. Thus, the nuclear spin selection rules are $\Delta I = 0$ for F transitions and $\Delta I = 0, 1$ ($0{-}0$ transitions are forbidden) for GT transitions. For the β decay with a change in the parity of nuclear states or a change in the nuclear spin by more than unity, the allowed matrix elements are zero; therefore, the dependence of β-transition operators on space coordinates and velocities of nucleons should be taken into consideration. These β transitions are called "forbidden transitions" and are commonly classified according to their degree of forbiddenness n (n-forbidden transitions), i.e., according to the sum of the powers of the coordinates and velocities of nucleons that appear in the β-transition operator. A change in the parity of nuclear states π is always $\pi = (-1)^n$. Transitions with the multipolarity $\lambda = n + 1$ are called "unique n-forbidden transitions".

When nuclei undergo the β decay, the Coulomb energy of the electron inside the nucleus is often high in comparison with the transition energy ΔE and the electron mass m_e at rest (ξ approximation). The Coulomb energy is represented by the dimensionless parameter ξ

$$\xi = (Ze^2)/(2Rm_ec^2) \approx 1.2ZA^{-1/3}, \tag{1}$$

which is a function of the nuclear radius R and charge Z, and the conditions of the ξ approximation (or the Coulomb approximation) are written as

$$\xi \gg \Delta E/m_ec^2, \quad \xi \gg 1. \tag{2}$$

In some occasions, the probability of the β transition can be represented as a product of the lepton part, described by the Fermi function, and the nuclear part, described by the strength function [4, 6, 11], and the β transition strength function $S_\beta(E)$ is only distinguished in the following cases: for allowed β transitions, for FF transitions in the ξ approximation, for unique n-forbidden transitions.

The strength function $S_\beta(E)$ governs the nuclear excitation energy (E) distribution of elementary charge-exchange excitations and their combinations like proton particle (πp)–neutron hole (νh) coupled to the moment J^π: $[\pi p \otimes \nu h]_{J^\pi}$ and neutron particle (νp)–proton hole (πh) coupled to the moment J^π: $[\nu p \otimes \pi h]_{J^\pi}$. The strength function of Fermi-type β transitions takes into account excitations $[\pi p \otimes \nu h]_{0^+}$ or $[\nu p \otimes \pi h]_{0^+}$. Since isospin is a quite good quantum number, the strength of Fermi-type transitions is concentrated in the IAR region. The strength function for β transitions of the Gamow–Teller type describes excitations $[\pi p \otimes \nu h]_{1^+}$ or $[\nu p \otimes \pi h]_{1^+}$. For FF β transitions in the ξ approximation, the significant configurations are $[\pi p \otimes \nu h]_{0^-,\,1^-}$ or $[\nu p \otimes \pi h]_{0^-,\,1^-}$. Residual interaction can cause collectivization of these configurations and give rise to resonances in $S_\beta(E)$. The positions and intensities of resonances in $S_\beta(E)$ are calculated within various microscopic models [7, 24]. From the macroscopic point of view, the resonances in the GT β-decay strength function $S_\beta(E)$ are connected with the oscillation of the spin–isospin density without change in the shape of the nucleus [4, 11, 14].

Level occupancy after the β decay $I(E)$, the half-life $T_{1/2}$, and ft values are related to $S_\beta(E)$ by the following equations [4, 21, 22]:

$$d(I(E))/dE = S_\beta(E)\, T_{1/2}\, f(Q_\beta - E), \tag{3}$$

$$(T_{1/2})^{-1} = \int S_\beta(E)\, f(Q_\beta - E)\, dE, \tag{4}$$

$$\int\limits_{\Delta E} S_\beta(E)\, dE = \Sigma_{\Delta E} 1/(ft), \tag{5}$$

where $S_\beta(E)$ is represented in units $\mathrm{MeV}^{-1} \cdot \mathrm{s}^{-1}$, and ft — in seconds.

The reduced probabilities of GT transitions $B(\mathrm{GT}, E)$ are related [4, 21–23] with ft, g_V and g_A values as

$$B^{\pm}(\mathrm{GT}, E) = ((g_{A\mathrm{eff}})^2/4\pi)|\langle I_f||\Sigma t_\pm(k)\sigma(k)||I_i\rangle|^2/(2I_i + 1), \tag{6}$$

$$B^{\pm}(\mathrm{GT}, E) = [D(g_V^2/4\pi)]/ft, \tag{7}$$

and for FF transitions, as

$$[B(\lambda^\pi = 2^-)] = 3/4 D g_V^2/(4\pi \cdot ft), \tag{8}$$

$$[B(\lambda^\pi = 0^-) + B(\lambda^\pi = 1^-)] = D g_V^2/(4\pi \cdot ft), \tag{9}$$

where I_i and I_f are the spins of the initial and final states; g_A and g_V are the constants of the axial-vector and vector components of the β decay; $D = (6144 \pm 2)$ s; $t_\pm(k)\sigma(k)$ is the product of the isospin and spin

operators giving the respective operators of the Gamow–Teller β transitions; ft is the reduced half-live of the β decay to the level with the excitation energy E; $\langle I_f||\Sigma t_{\pm}(k)\sigma(k)||I_i\rangle$ is the reduced nuclear matrix element for the Gamow–Teller transition.

The conserved vector-current (CVC) hypothesis and partially conserved axial-vector-current (PCAC) hypothesis yield the free-nucleon [25] value $g_{A\text{free}}/g_V = -1.2723(23)$. Inside nuclear matter, the effective value $g_{A\text{eff}}$ is needed to reproduce experimental observations. Precise information on the value of $g_{A\text{eff}}$ is crucial [25] when predicting half-life for β decays, β-decay strength function for GT and FF β transitions, and cross section for charge-exchange reactions. The effective value of $g_{A\text{eff}}$ is characterized by a renormalization factor q (in the case of quenching of g_A, it is called "a quenching factor"): $q = g_{A\text{eff}}/g_{A\text{free}}$, where $g_{A\text{eff}}$ is the value of the axial-vector coupling derived from a given theoretical or experimental analysis. The experimental methods of quenching value determination in many cases may have essential uncertainties [25]. One of the model-independent methods for $g_{A\text{eff}}$ determination [21, 22, 25] is the comparison of the experimental total GT β-decay strength with the Ikeda sum rule. For application of this method, it is necessary to have the total GT strength in the energy window allowed for the β decay, and contribution from non-nucleonic degrees of freedom (Δ-isobar, for example) must be neglectable. Such situation may be realized [21, 22] for the β decay of halo nuclei (^{6}He, ^{11}Li) or for very neutron-rich nuclei, where the Gamow–Teller resonance energy E_{GTR} is less than the isobar-analog resonance energy E_{IAR}. It is well known that the GT total strength satisfies the Ikeda sum rule, which is written as

$$S^- - S^+ = 3(N - Z), \tag{10}$$

$$S^{\pm} = \Sigma_f |\langle I_f||\Sigma\, t_{\pm}(k)\, \sigma(k)||I_i\rangle|^2/(2I_i + 1), \tag{11}$$

$$\Sigma_j\, B^-(\text{GT}, E_j) - \Sigma_k\, B^+(\text{GT}, E_k) = 3(N - Z)(g_{A\text{eff}})^2/4\pi, \tag{12}$$

where $B^-(\text{GT}, E_j)$ and $B^+(\text{GT}, E_k)$ are determined from (6) for charge-exchange processes of the GT type and from (7) for the GT β^- or β^+/EC decay. When $S^+ \approx 0$ or $S^+ \ll S^-$, for the β^- decay, one obtains

$$\Sigma j\; D/ft_j = 3(N - Z)(g_{A\text{eff}}/g_V)^2, \tag{13}$$

and from β^--decay data, one can estimate for mother nucleus the ratio $(g_{A\text{eff}}/g_V)^2$ or the quenching factor q_{GT}.

The scheme of levels that are significant for analyzing the strength functions for the Gamow–Teller transitions is shown in Fig. 2. In the β^+/EC decay of $N > Z$ nuclei, there is only one isospin value of $T_0 + 1$ in coupling the isospin ($\tau = 1$, $\mu_\tau = +1$) of the $[\nu p \otimes \pi h]_{1^+}$ configuration to the neutron-excess isospin T_0. The most collective state formed by $[\nu p \otimes \pi h]_{1^+}$ excitations characterized by the isospin $\tau = 1$ and the isospin projection $\mu_\tau = +1$ is also referred to [4] as a $\mu_\tau = +1$ Gamow–Teller resonance. For the β^- decay of $N > Z$ nuclei, the Gamow–Teller resonance ($\tau = 1$, $\mu_\tau = -1$) lies (Fig. 2) at excitation in the IAR region and at the GTR energies typically in excess

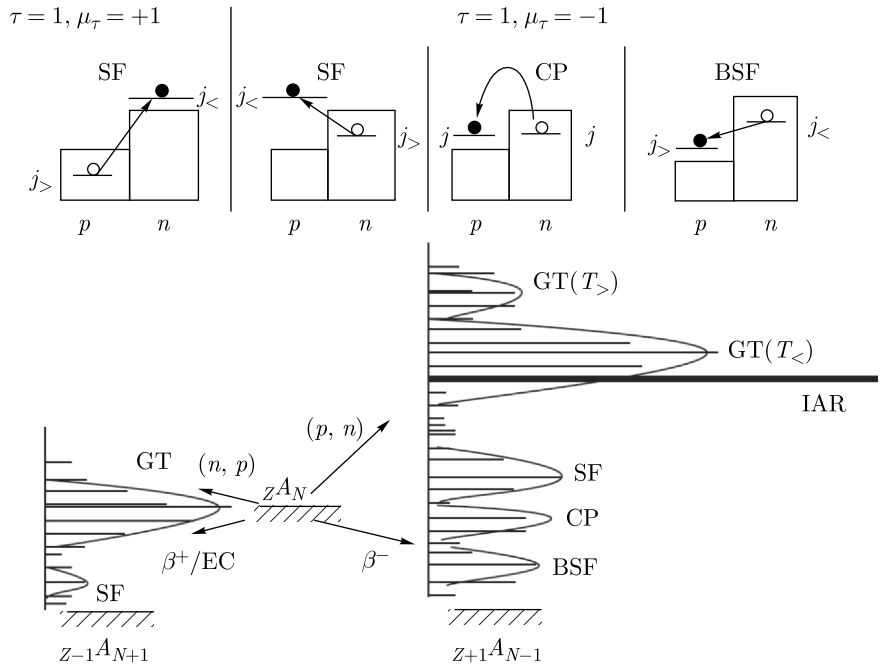

Fig. 2. Diagram of strength functions for GT β transitions and configurations that form resonances in $S_\beta(E)$ for GT transitions. The strength of the Fermi-type transitions is concentrated in the IAR region

of Q_β, and GTR is usually energetically inaccessible to population in the β^- decay, but the $\mu_\tau = +1$ Gamow–Teller resonance can be populated by the β^+/EC decay [4, 6, 11]. In nuclei with $Z > N$, the situation reverses for the β^- and β^+/EC decays.

Strength functions for the β^- and β^+/EC transitions are qualitatively different, which is manifested primarily in the total sum of the β^- and β^+/EC transitions. According to the sum rule (10) for nuclei with $N > Z$, the total sum of the β^- transitions is substantially larger than that of the β^+/EC transitions. However, this does not mean that the reduced half-lives log ft for the β^- and β^+/EC transitions between low-lying states should greatly differ. It is evident from the scheme in Fig. 1 that far from all, the states contributing to the total sums $S^\pm$ fall within the energy window $E < Q_\beta$ in the β^- and β^+/EC decays. It is known [4, 6, 11] that for nuclei with $N > Z$, more than 90% of the total strength of GT β^- transitions are concentrated in the Gamov–Teller resonance, which, as a rule, is located much higher in excitation energy than the β^--decay energy Q_β (Figs. 1 and 2), meaning that the forces corresponding to the total sums S^- and S^+ can be comparable in the low excitation energy region. Differences in β^-- and β^+/EC-decay strength functions only slightly affect the probabilities for the β^- and β^+/EC

transitions in nuclei near the β-stability line. These differences become more pronounced as the distance from the β-stability line and total β-decay energy Q_β increase.

The previously dominant statistical model assumed that there were no resonances in $S_\beta(E)$ and the relations $S_\beta(E) = \text{const}$ or $S_\beta(E) \sim \rho(E)$, where $\rho(E)$ is the level density of the daughter nucleus, were considered to be a good approximation for medium and heavy nuclei [26]. Investigations of the β-delayed processes and experiments on measurements of $S_\beta(E)$ by using total absorption gamma spectroscopy (TAGS) unambiguously revealed the nonstatistical character of $S_\beta(E)$ for the GT-type β decay and stimulated the development of microscopic models making it possible to use the structure of the atomic nucleus for calculating $S_\beta(E)$ [4, 6, 7]. The next step was done [11–14] by application of high-resolution nuclear spectroscopy techniques for $S_\beta(E)$ fine stricture study. These techniques made it possible to unambiguously demonstrate the resonance structure of $S_\beta(E)$, not only for GT transitions but also for FF β transitions [11–13]. It was experimentally shown that for some excitation energies of daughter nuclei, the probability of FF β^+/EC transitions is comparable with that of GT β^+/EC transitions. It is due to high-resolution spectroscopy techniques that the resonance structure of $S_\beta(E)$ for FF transitions was first revealed [11–13]. The high-resolution nuclear spectroscopy techniques made it possible to observe the splitting of the resonance in $S_\beta(E)$ for the β^+/EC decay of the deformed nuclei into two components. This splitting is thought to be associated with anisotropy of the isovector density oscillation in deformed nuclei [11, 14].

Theoretical description of the β-transition strength function structure at the microscopic level is intimately connected with analysis of astrophysical and thermonuclear processes, description of $\log ft$ for β transitions between low-lying states of atomic nuclei, analysis of delayed processes, study of charge-exchange processes, and some other nuclear physics problems [1–6, 11]. One of the first calculations of the microscopic structure of $S_\beta(E)$ for GT β transitions which accounted for shell effects and spin–isospin residual interaction and enabled an explanation for the delayed fission was performed in [1–4]. At the present time, the existing theory allows us to calculate quite correctly the positions and relative intensities of the peaks in the strength functions for Gamow–Teller transitions [7, 11, 24]. Even for spherical nuclei, the deviation of the calculated absolute intensities of the strength function peaks from their experimental counterparts is as large as a few tens of percent to a few hundred percent, the theory predicting more intense peaks than those observed experimentally [4, 6, 7, 24, 25].

Strong mixing of configurations for high excitation energies and level densities should cause the resonance structure to disappear in the strength functions $S_\beta(E)$. The approximate symmetry of nuclear interaction prevents some configurations from mixing. For configurations populated by GT $\beta^-$and β^+/EC transitions, mixing is weaker because of partial $SU(4)$ spin–isospin symmetry of interaction in the nucleus [4, 6, 11, 21, 22]. For FF β^- and β^+/EC transitions, the resonance structure is also observed in the strength

function $S_\beta(E)$ [11–13]. The resonance structure in the strength function for FF β^- and β^+/EC transitions can indicate partial symmetry of interaction in the nucleus which corresponds to the first forbidding. This means that configurations populated by FF transitions are also distinguished in approximate quantum numbers between neighboring levels of the daughter nucleus, and no strong configuration mixing occurs.

2. INVESTIGATION OF THE β-DECAY STRENGTH FUNCTIONS STRUCTURE BY THE TOTAL ABSORPTION GAMMA SPECTROSCOPY

Fermi function $f(Q_\beta - E)$ decreases with excitation energy E increasing and, as a rule (Fig. 1), the more intensive β decays populate the levels with low (less than 2–3 MeV) excitation energies. But from the nuclear structure point of view, the most interesting β transitions populate the levels with high (more than 2–4 MeV) excitation energies where in $S_\beta(E)$ the resonances or their tails may be observed. To obtain information about the $S_\beta(E)$ structure, it is necessary to measure the level populations after the β decay. A TAGS method of direct measurement of the level population probabilities in the β decay was proposed in [27]. A principle of this method is that the γ rays accompanying the β decay are detected by the large NaI crystal in a nearly 4π geometry. If the efficiency of total absorption of γ rays is sufficiently high, the pulse height in such total absorption spectrometer (TAS) is determined by the total energy of γ rays, i.e., by the energy of the level populated by the β transition. At the same time, special measures must be taken to shield the crystals from the β particles entering them. But the constructed spectrometer [27] has the solid angle about 80%, and the detection efficiency for the total absorption peak for a cascade of γ rays depends on the scheme of γ transitions and on the number of γ rays in the cascade (multiplicity). Applications of the first total absorption spectrometers [27] did not allow the authors to identify a nonstatistical resonance character of $S_\beta(E)$. As a result, it was wrongly assumed that both the β decay and the γ deexcitation of the levels are statistical in nature, and some observed "resonances" were interpreted as the statistical fluctuations. Considering the fundamental importance of direct measurement of β-decay strength functions, conditions for the possibility of using TAS to obtain β-transition strength functions in a wide excitation energy interval were formulated in [4, 6]. On the basis of this analysis, a spectrometer with practically 4π geometry has been built (Fig. 3) and successfully used to demonstrate the resonance structure of $S_\beta(E)$ [4, 6, 7, 11]. The results of some of the first successful applications of the TAGS spectrometer for measuring the resonance structure of $S_\beta(E)$ are summarized in [4, 6, 7, 11, 28].

It was found [4, 6, 11] that the total absorption efficiency ε_{tot} is exponentially dependent in the energy range of 0.1–4.5 MeV on the total cascade γ-transition energy $E\gamma$:

$$\varepsilon_{\text{tot}} = \exp(-\alpha E\gamma), \quad \alpha = 0.78(3)\ \text{MeV}^{-1}. \tag{14}$$

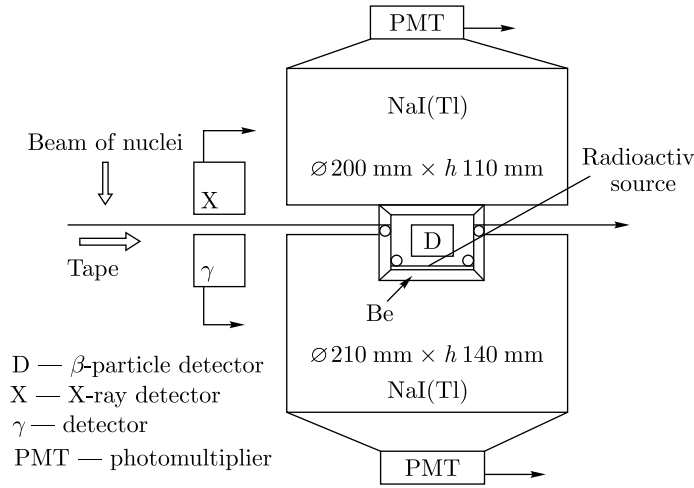

Fig. 3. General diagram of the detection part of the total absorption γ-ray spectrometer [7, 11] for investigation of β-decay strength functions

If relation (14) holds true, the intensity of the total cascade γ-ray absorption peak is proportional to the probability for population of a particular level in the daughter nucleus by the β decay and does not depend on the decay scheme. Indeed, if we have a deexcitation scheme for a level with energy E populated by the β decay, then, if relation (14) holds true, the detection efficiency for the total absorption peak for a cascade of N γ rays with the total energy $E = E\gamma_1 + \ldots + E\gamma_N$ is defined as

$$\varepsilon_{\text{tot}}(E) = \exp(-\alpha E\gamma_1) \times \ldots \times \exp(-\alpha\ E\gamma_N) = \\ = \exp(-\alpha(E_{\gamma 1} + \ldots E\gamma_N)) = N\ \exp(-\alpha E) \quad (15)$$

and does not depend on the scheme of γ transitions. Conversion of γ radiation introduces a systematic error into the analysis of total absorption spectra, and it can be difficult to take this error into consideration. Validity of (14) is substantially important for TAS and requires experimental verification. It is also important that 4π geometry of the TAGS spectrometer is maintained. Indeed, if the detection solid angle Ω for the cascade of N γ rays is different from 4π, the total absorption efficiency will be defined not by (15) but by the relation

$$\varepsilon_{\text{tot}}(E) = (\Omega/4\pi)^N \exp(-\alpha E), \quad (16)$$

i.e., it will strongly depend on the decay scheme (multiplicity N).

Until recently, experimental investigations of the $S_\beta(E)$ structure were carried out using total absorption gamma-ray spectrometers (TAGS) and total absorption spectroscopy methods, which had low energy resolution. With TAGS spectroscopy, it became possible to demonstrate experimentally (Figs. 4–6) the nonstatistical resonance structure of $S_\beta(E)$ for Gamow–Teller

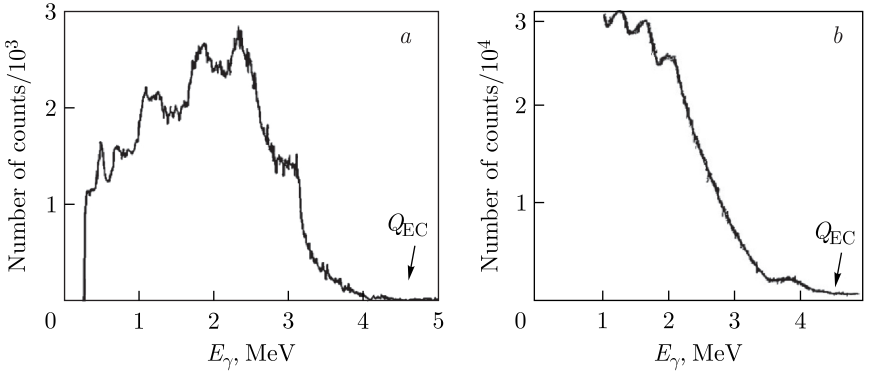

Fig. 4. Spectra of γ rays from the β^+/EC decay of ^{147g}Tb measured by TAGS in coincidence with particles (*a*) and without coincidence (*b*). The arrow points to the total electron capture energy Q_{EC} for ^{147g}Tb

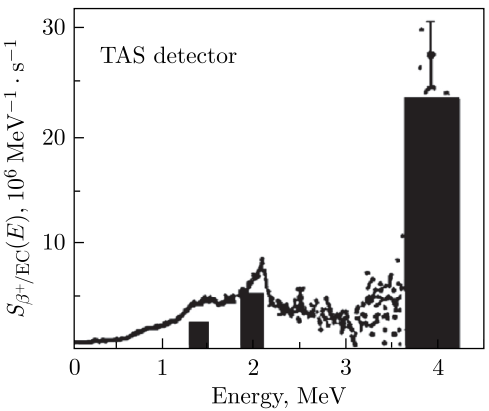

Fig. 5. Strength function $S_\beta(E)$ for the β^+/EC decay of ^{147g}Tb obtained from the analysis of the TAGS γ-ray spectra from the β^+/EC decay of ^{147g}Tb. The highest-intensity peak in the excitation energy region $E \approx 4$ MeV is interpreted as a tail of the GT resonance with $\mu_\tau = +1$

β transitions [4, 6, 7, 11]. There are two methods of the TAGS spectra analysis. In the first one [4, 7, 11], it is necessary to identify the total absorption peaks in TAGS spectra and have the 4π spectrometer with exponential energy dependence of the total absorption efficiency (i.e., the ratio of the number of pulses in the total absorption peak to the number of γ rays incident on the detector) for γ-ray registration. Only in this case, the efficiency of TAGS peak registration does not depend on the details of the decay scheme. This method gives good results, but can be applied for nuclei with total β-decay energy Q_β less than 5–6 MeV. Quantitative characteristics may be obtained, as a rule, only for one peak (β^- decay) and for two peaks (β^+/EC decay) in $S_\beta(E)$. The second method [8–10] is based on the so-called response function application, but much assumption must be done for extraction of the $S_\beta(E)$ shape from the TAGS spectrum shape. Analysis depends on the assumptions about the decay scheme which generally is not known. It is very difficult to

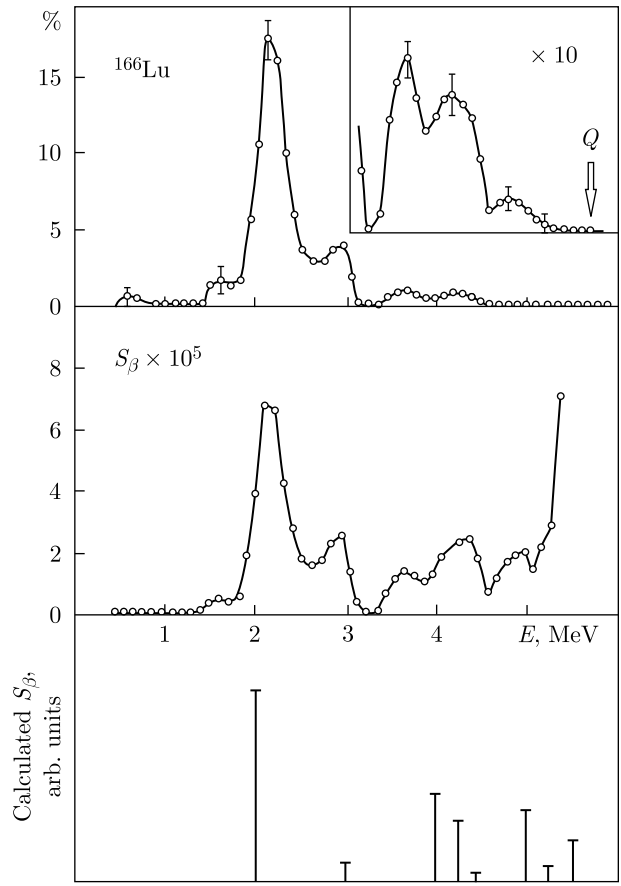

Fig. 6. Level population probabilities, $S_\beta(E)$ for the β^+/EC decay of ^{166}Lu obtained by TAGS, and results of calculation of β^+/EC-decay probabilities with the Gamow–Teller (spin–isospin) residual interaction [4]

estimate the associated systematic errors and uncertainties of such analysis and only qualitative information about $S_\beta(E)$ may be obtained. The conversion electrons are not measured by TAGS and it is advisable to evaluate the associated systematic error for both methods of the TAGS spectra analysis.

In this review, we applied the first method for the TAGS spectra analysis [4, 7, 11]. The TAGS spectrometer is schematically shown in Fig. 3. Its γ-ray detection efficiency ε_{tot} in the total absorption peak in the excitation energy range investigated by the author in ^{147}Gd daughter nuclei (0.1–4.6 MeV) exponentially depends on the total energy E_γ of the deexcitation γ transitions [7]. It is known [4, 11] that in this case, the intensity of the total γ-ray absorption peak is proportional to the level population probability in

the β decay and does not depend on the decay scheme. Therefore, the analysis of the measured spectra was reduced to revealing total γ-ray absorption peaks and determining their intensities. Next, the strength function for the β^+/EC decay of ^{147g}Tb was constructed (Figs. 4 and 5) using the thus obtained intensities of the total γ-ray absorption peaks and relation (3).

The γ-ray spectra measured with the total absorption spectrometer in coincidence with the β^+ particles at the β^+/EC decay of ^{147g}Tb and without coincidence are shown in Fig. 4. The end-point energy of the total absorption spectra is determined by the total electron capture energy $Q_{\mathrm{EC}} = 4.6$ MeV. The peak with the energy $E_\gamma \approx 4$ MeV in the spectrum without coincidence and the peak at $E_{\gamma'} \approx 3$ MeV in the coincidence spectrum have the maximum energies and are identified as the total absorption peaks. The peak at $E_\gamma \approx$ $\approx E_{\gamma'} - 2m_e c^2 \approx 2$ MeV in the spectrum without coincidence, where $2m_e c^2$ is the energy of two annihilation quanta, corresponds to the total absorption peak at $E_{\gamma'} \approx 3$ MeV. So, the peak at $E_\gamma \approx 2$ MeV in the spectrum without coincidence is also the total absorption peak. Thus, two peaks at the energies of 4 and 2 MeV can be reliably identified in the strength function for the β^+/EC decay of ^{147g}Tb (Figs. 4 and 5), and no information on the decay scheme is needed for finding the intensities and energies of these two peaks during the analysis of the total absorption γ spectra. In $S_\beta(E)$ for ^{147g}Tb, a third peak is observed at $E \approx 1.4$ MeV, but reliable determination of its intensity requires information on the deexcitation scheme of excited levels in ^{147}Gd, due to difficulties in identifying the total absorption peak in this energy region. Note that two total absorption peaks can be identified for the β^+/EC decay in the TAGS spectra. This is possible when the total absorption peak with the highest energy falls within the energy window accessible for electron capture but inaccessible for the β^+ decay. In Fig. 5, the intensity of the peak with the energy $E \approx 1.4$ MeV in $S_\beta(E)$ was obtained from the analysis of the total γ-ray absorption spectra under the assumption that levels in the excitation energy region $E \approx 1.4$ MeV are deexcited through emission of two γ rays with equal energies. Thus, it is possible to reliably determine the energy and intensity of two peaks with the energies $E \approx 4$ and 2 MeV in the strength function for the β^+/EC decay of ^{147g}Tb (Fig. 5). The highest-intensity peak in the excitation energy region $E \approx 4$ MeV is interpreted as the tail of the main GT resonance [7] with $\mu_\tau = +1$ (according to the scheme for $S_\beta(E)$, Fig. 2).

Theoretical calculations [7] performed within the MQPM model with the QRPA approach revealed, like the experiment, the highest-intensity peak in $S_\beta(E)$ (GT resonance with $\mu_\tau = +1$) in the excitation energy region $E \approx 4$ MeV of the ^{147}Gd daughter nucleus. This allows for the conclusion that the above model is applicable to the description of $S_\beta(E)$ for spherical nuclei to which the ^{147g}Tb nucleus under investigation and its daughter nucleus ^{147}Gd belong. Note, however, that theoretical calculations [7] yield the intensity of the main resonance with the energy $E \approx 4$ MeV several times higher than the experimental value. This "big overestimation" can result from the fact that in the experiment, we observe only that part of the resonance which falls

within the energy region accessible for electron capture. However, theoretical calculations [4, 7, 24] typically correctly describe the energy but give a higher intensity of resonances (Fig. 6) than that observed experimentally. This (quenching factor) is characteristic of many nuclei investigated by the TAGS technique [4, 28, 29].

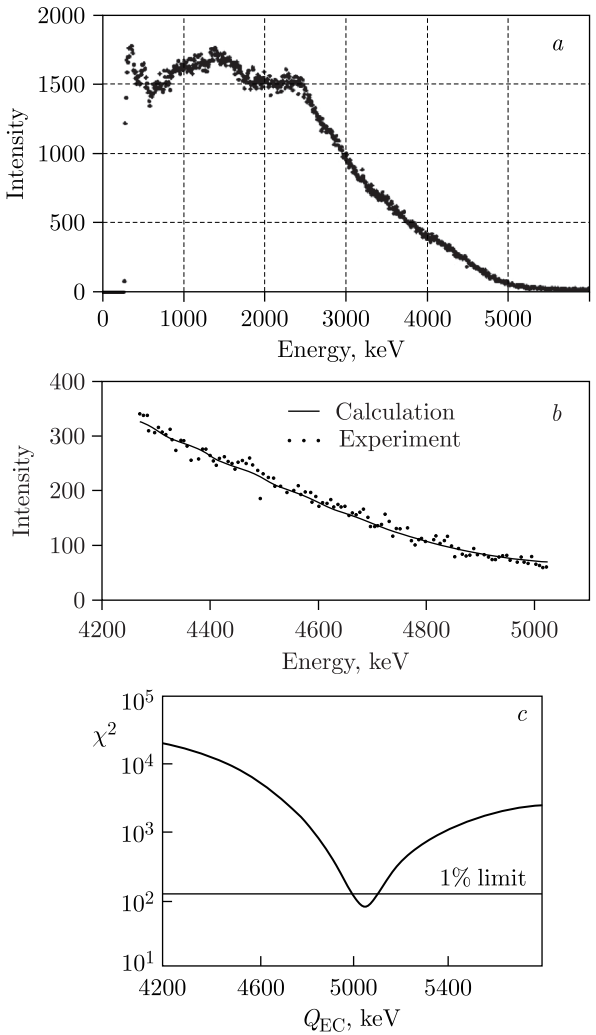

Fig. 7. Experimental TAGS spectra (*a*) and fitted range of TAGS spectra (*b*) of ^{156}Ho ($T_{1/2} \approx 56$ min), $Q_{EC} = (5.05 \pm 0.07)$ MeV. The number of degrees of freedom for the fitted range is $\nu = 105$, $\chi^2_{min}/\nu = 0.81$ (*c*)

Thus, the TAGS techniques allow the resonance character of $S_\beta(E)$ to be revealed and data on the $S_\beta(E)$ structure to be obtained when total absorption peaks are reliably identified in the TAGS spectrum. It is usually one total absorption peak that is identified in $S_\beta(E)$ for the β^- decay and two peaks in $S_\beta(E)$ for the β^+/EC decay. To obtain more comprehensive information on the $S_\beta(E)$ structure, one should use high energy-resolution nuclear spectroscopy techniques [7, 11–15].

The end point of the TAS spectrum is connected with the total energy Q_β of the β decay. TAGS spectroscopy can be used for measurements of Q_β with accuracy up to 50 keV [4]. As a rule, the most informative region for determination of the TAGS spectrum end point has a low counting per channel and determining it directly is very difficult. The part of the TAGS spectrum with sufficiently high statistics is not so informative for this purpose. So, there is an optimal interval of the TAS spectrum for determination of Q_{EC}. We use the χ^2 criterion for selecting the optimal energy interval [15]. In the fitted region, the errors of the intensity determination δI exceeded the maximum value of the pileup spectrum intensity. The results of determination of Q_{EC} from TAS spectra of the β^+/EC decay of ^{156}Ho ($T_{1/2} \approx 56$ min) are presented in Fig. 7. The obtained value $Q_{\mathrm{EC}} = (5.05 \pm 0.07)$ MeV for ^{156}Ho ($T_{1/2} \approx 56$ min) is in good agreement with the systematics [15, 29].

Since the conversion electrons are generally not detected and at $E_\gamma > 5$ MeV there is no exponential dependence of the total absorption efficiency on E_γ, the TAGS spectra analysis may give incorrect result. Also, TAGS cannot distinguish the GT and FF transitions and may offer only limited information about $S_\beta(E)$. However, using TAGS, one can determine the total energy Q_β of the β decay [4, 6, 11, 15], demonstrate the resonance structure of $S_\beta(E)$, in combination with high-resolution nuclear spectroscopy methods give the quantitative information about $S_\beta(E)$ both for GT and FF β decays and identify the degree of incompleteness of the decay scheme.

3. HIGH-RESOLUTION γ SPECTROSCOPY AND FINE STRUCTURE OF THE β-DECAY STRENGTH FUNCTIONS

TAGS methods have some disadvantages arising from poor energy resolution of NaI-based spectrometers. Only one or two absorption peaks can be identified in TAGS spectra, isobaric impurities in the analyzed source often give rise to uncertainties, thus, it is impossible to discriminate between GT and FF β transitions and to measure the fine structure of $S_\beta(E)$; difficulties often emerge in spectrum processing, namely, when it is necessary to consider the internal conversion of γ rays or to identify total absorption peaks. Exponential dependence [4, 11] of the TAGS efficiency from the energy is substantially important for the total absorption spectrometer and requires experimental verification in the range of energies up to Q_β. Therefore, it is quite important to measure $S_\beta(E)$ using high-

resolution γ-spectroscopy techniques. Development of experimental techniques allows application of methods of nuclear spectroscopy with high energy resolution (including high-resolution γ spectroscopy and conversion electron spectroscopy) for the $S_\beta(E)$ fine structure measurement. The results of some of the first successful measurements of the $S_\beta(E)$ fine structure are summarized in [11, 12]. Combination of the total absorption spectroscopy with high-resolution spectroscopy may be applied to the detailed decay schemes construction [7, 11, 15]. High-resolution nuclear spectroscopy methods [11–13] made it possible to demonstrate experimentally the resonance nature of $S_\beta(E)$ for first-forbidden β transitions and reveal splitting of the peak in $S_\beta(E)$ for the GT β^+/EC decay of the deformed nuclei into two components. This splitting indicates anisotropy of isovector density component oscillation [11, 14].

Using our TAGS spectrometer, we observed [7, 11] the tail of the Gamow–Teller resonance with $\mu_\tau = +1$ (Fig. 5) in ^{147g}Tb ($T_{1/2} \approx 1.6$ h) as a strong peak at $E \approx 4$ MeV. The β^+/EC transitions to the levels with excitation energies higher than 2 MeV were not identified in the decay scheme (Fig. 8) from [29]. This means that the decay scheme of ^{147g}Tb in [29] is strongly incomplete. The more complete decay scheme of ^{147g}Tb was constructed in [30] (Fig. 9). The most interesting region for studying the

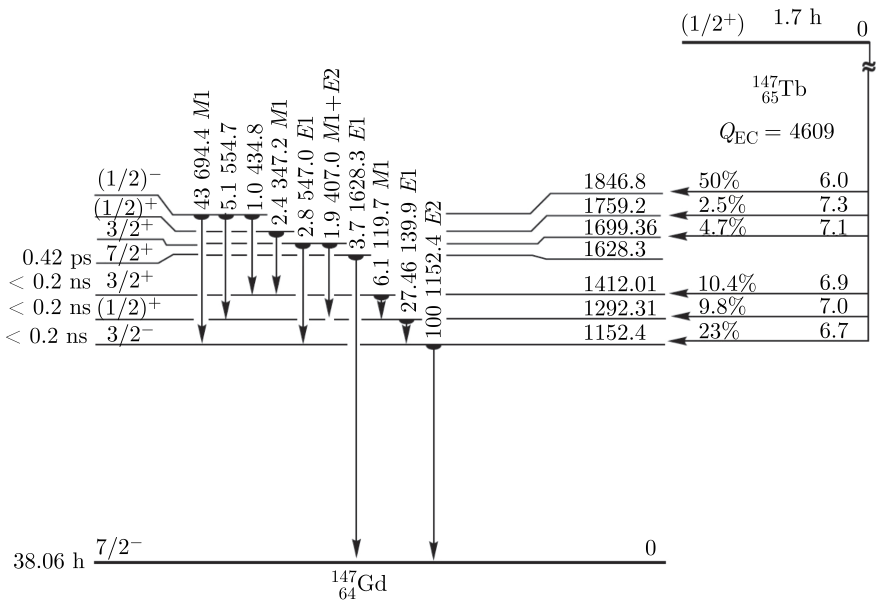

Fig. 8. ^{147g}Tb decay scheme from [29]. The β^+/EC transitions to the region where the excitation energy is higher than 2 MeV are not indicated. This decay scheme is not complete and does not agree with TAGS data. (Level energies and $Q_{\rm EC}$ are in keV.)

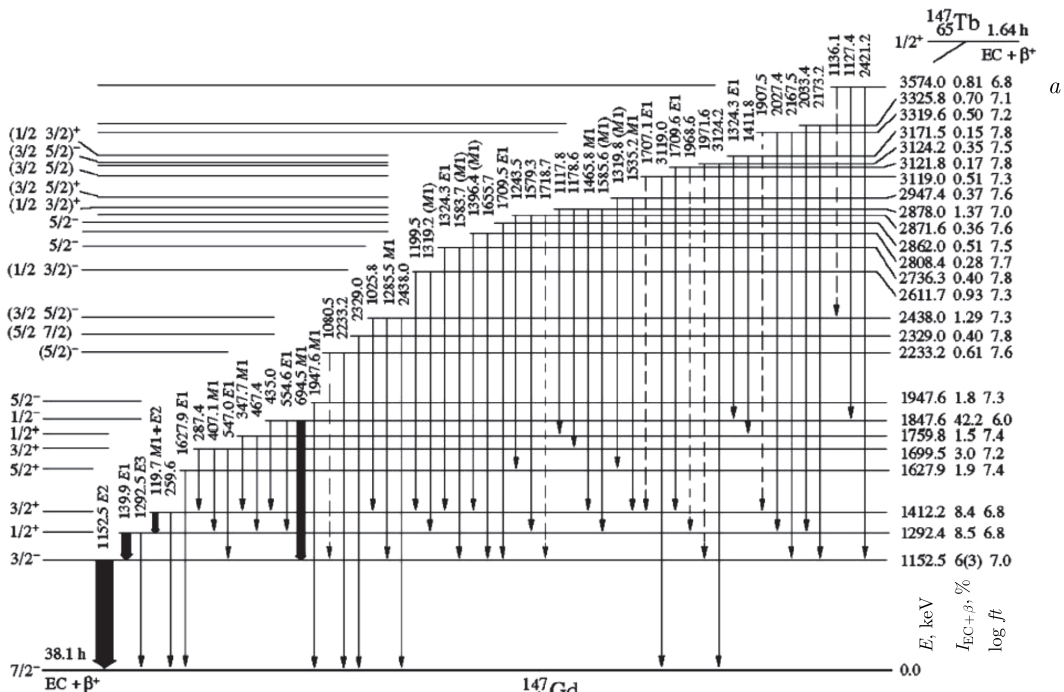

Fig. 9*a*. ^{147g}Tb decay scheme from [29]. *a*) Low energy levels of ^{147}Gd; *b*) high energy levels of ^{147}Gd. There are many β^+/EC transitions to the region where the excitation energy is higher than 2 MeV. This decay scheme is quite complete as it is in good agreement with TAGS data

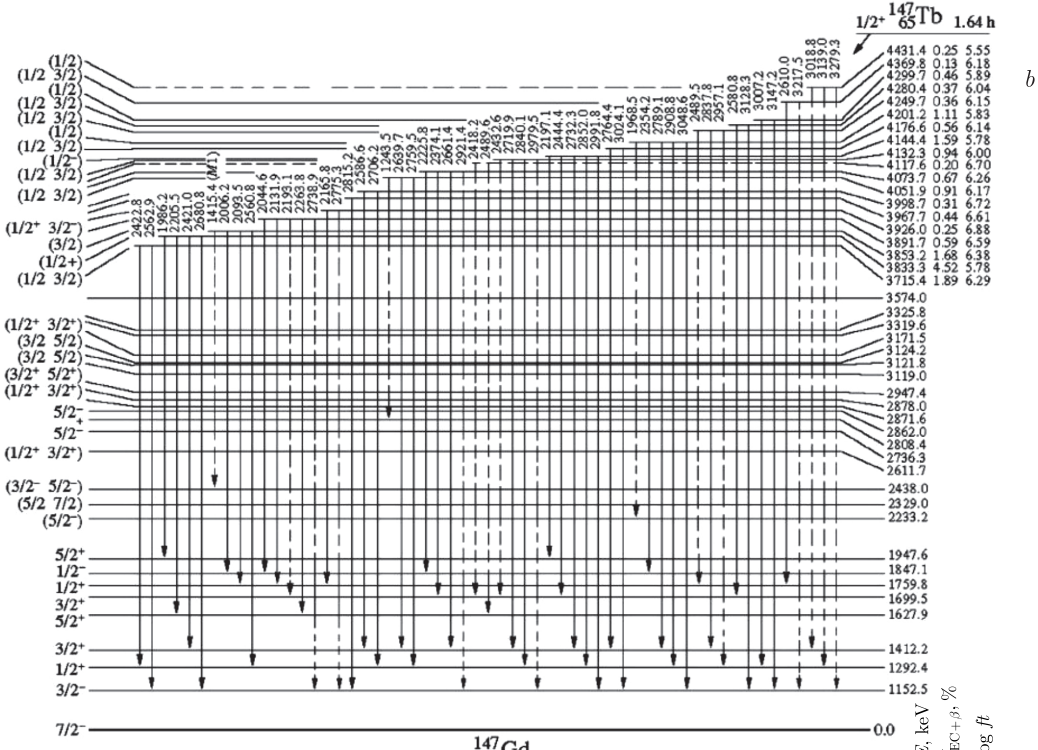

Fig. 9*b*.

b

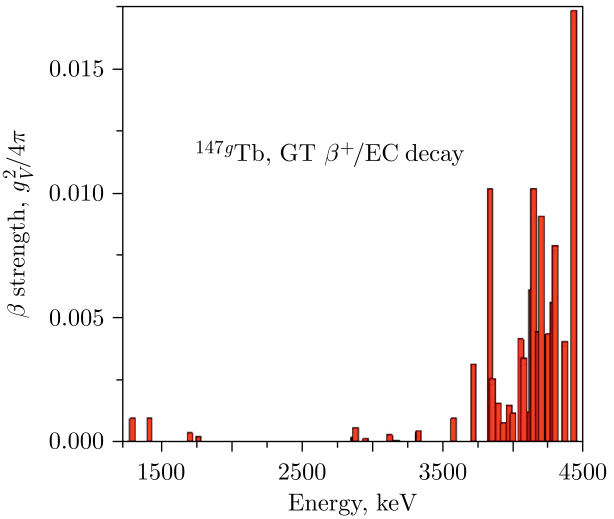

Fig. 10. Fine structure of the GT β^+/EC-decay strength functions [11, 12] for spherical nuclei ^{147g}Tb deduced from the quite complete (Fig. 9) decay scheme [30]

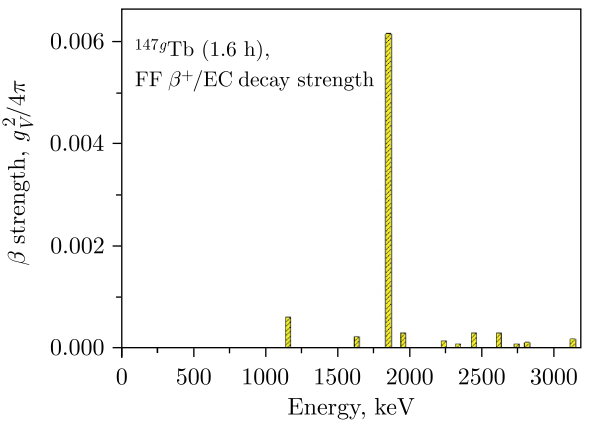

Fig. 11. Fine structure of the FF β^+/EC-decay strength functions [11, 12] for spherical nuclei ^{147g}Tb deduced from the quite complete (Fig. 9) decay scheme [30]

β-strength function is at an excitation energy higher than 2–4 MeV. The β^+/EC-decay strength function (Figs. 10 and 11) deduced from the more complete decay scheme was constructed in [11, 12]. The strength functions (Figs. 5 and 10) are in good agreement and one may conclude that the scheme of ^{147g}Tb β^+/EC decay in [30] is sufficiently complete. This demonstrates that the decay schemes for transitions to the levels with excitation energies higher than 2–3 MeV in medium and heavy nuclei may be very incomplete.

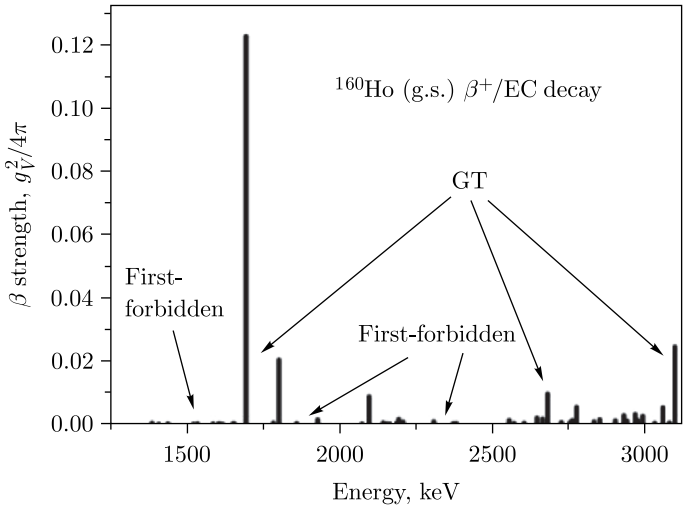

Fig. 12. Fine structure of the strength functions for deformed nuclei ^{160}Ho ground state (g.s.) GT and FF β^+/EC decays ($T_{1/2} = 25.6$ min, $Q_{\text{EC}} = 3.3$ MeV) [11, 12]

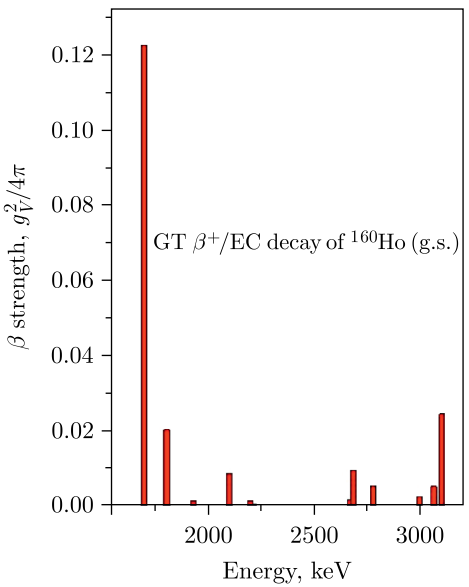

Fig. 13. Fine structure [11–14, 31] of the g.s. GT β^+/EC-decay strength function for deformed nuclei ^{160}Ho

For detailed decay scheme construction and $S_\beta(E)$ fine structure study, it is necessary to have much more time for measurements and data analysis compared with TAGS experiments.

From the macroscopic point of view, the resonances in the GT β-decay strength function $S_\beta(E)$ are connected with the oscillation of the spin–isospin density without change in the shape of the nucleus [4, 14, 31]. Intensities of K-allowed β transitions to the levels of the same rotational band and intensity ratios of electromagnetic transitions inside the band and between the states of different bands satisfy simple relations following from the rotational model (Alaga rules) [32]. The ft ratios at $|K_i - K_f| \leqslant \lambda$ and $|K_i + K_f| > \lambda$ are expressed in terms of the ratios of the squares of the corresponding Clebsch–Gordan coefficients:

$$ft(I_iK_i \to I_{1f}K_f)/ft(I_iK_i \to I_{2f}K_f) = \\ = \langle I_iK_i\lambda K_i - K_f|I_{2f}K_f\rangle^2/\langle I_iK_i\lambda K_i - K_f|I_{1f}K_f\rangle^2, \quad (17)$$

where λ is the β-transition multipolarity ($\lambda = 1$ for GT β transitions). If $|K_i + K_f| \leqslant \lambda$ and $K_{i,f} \neq 0$, contributions from the signature-involving terms must be taken into consideration [31]. Obeyance of this rule means that the wave functions of the rotational band levels do not have impurity components of neighboring states and the adiabaticity condition is fulfilled. The results of the calculations by formula (17) and the experimental data are presented in Table 1. Considering the excitation energy and quantum characteristic of the levels, experimental data are in rather good agreement with the estimations by (17), which indicates correct balance of the ^{160g}Ho (25.6 min) decay scheme.

The average energy $\langle E\rangle$ of the $S_\beta(E)$ peak is calculated by formula

$$\langle E\rangle = \Sigma_i E_i \cdot ft_i^{-1}/\Sigma_i ft_i^{-1}. \quad (18)$$

Using the data from Table 2, we obtain for the γ-type spin–isospin oscillation (oscillations perpendicular to the symmetry axis) $\langle E\rangle_\gamma = 2737$ keV and for the β-type spin–isospin oscillation (oscillations along the symmetry

Table 1. **^{160}Dy levels populated by the ^{160g}Ho (25.6 min) GT β^+/EC decay and making the largest contribution to the intensity of the β component of the $S_\beta(E)$ peak**

Energy of the level, keV	Quantum (I^π; K^π) characteristics	Level population from the β^+/EC decay, % per decay	$\log ft$
1694.36(2)^^	$I^\pi = 4^+$; $K^\pi = 4^+$	74(5)	4.72(3)
1802.24(2)^^	$I^\pi = 5^+$; $K^\pi = 4^+$	10.8(9)	5.49(4)
1929.19(2)^^	$I^\pi = 6^+$; $K^\pi = 4^+$	0.62(7)	6.65(5)
2096.87(2)*	$I^\pi = 4^+$; $K^\pi = 4^+$	2.9(2)	5.86(3)
2194.43(3)*	$I^\pi = 5^+$; $K^\pi = 4^+$	0.43(3)	6.61(4)

Note. * and ^^ stand for the levels in the same rotational bands.

Table 2. **Ratios of ft for pairs of levels from the same band populated by the ^{160g}Ho (25.6 min) GT β^+/EC decay, $I^\pi = 5^+$, $K^\pi = 5^+$. Experimental and calculated data are given for two rotational bands in ^{160}Dy**

Energy of the level E_1, keV	Energy of the level E_2, keV	Experiment, $ft(E_1)/ft(E_2)$	Calculation by formula (17), $ft(E_1)/ft(E_2)$
1694.2	1802.2	0.16	0.11
1694.2	1929.1	0.012	0.018
1802.2	1929.1	0.07	0.16
2096.8	2194.4	0.17	0.11

axis) $\langle E\rangle_\beta = 1749$ keV. Thus, the splitting due to the anisotropy of the spin–isospin density oscillations $\langle E\rangle_\gamma - \langle E\rangle_\beta$ in the deformed ^{160}Dy nucleus is about 1 MeV. When the oscillations are along the symmetry axis, the projection of the angular momentum on the axis is zero ($\Delta K = 0$), the axial symmetry is not broken, and oscillations of this type do not lead to K-forbidding for GT β transitions. Oscillations perpendicular to the symmetry axis break the axial symmetry and have a nonzero projection of the angular momentum on the axis ($\Delta K = \pm 1$ for dipole oscillations, $\Delta K = \pm 2$ for quadrupole oscillations, etc.), which leads to K-forbidding for a number of β^+/EC transitions and a decrease in the intensity of the corresponding component of the peak in $S_\beta(E)$ (Figs. 12 and 13). A significant fact is that the amplitude of the higher-energy peak is much smaller than the amplitude of the lower-energy peak. This relationship of the peak amplitudes arises from K-forbidding of GT transitions for a prolate nucleus (quadrupole deformation parameter $\beta_2 > 0$). No similar splitting of the peak (Fig. 10) in $S_\beta(E)$ is observed in the GT β^+/EC decay of the spherical ^{147g}Tb nucleus [11, 31].

Charge-exchange particle-hole excitations populated by the β decay are related to the oscillation of the $\mu_\tau = \pm 1$ components of the isovector density [11, 31] $\rho_{\tau=1,\,\mu\tau}$:

$$\rho_{\tau=1,\,\mu\tau}(r) = \Sigma_k\, 2t_{\mu\tau}(k)\,\delta(r - r_k), \tag{19}$$

where the summation is taken over all nucleons k, and $t_{\mu\tau}$ is the spherical component of the nucleon isospin t:

$$t_{\mu\tau} = \begin{cases} (1/2)^{1/2}(t_x - it_y), & \mu_\tau = -1, \\ t_z, & \mu_\tau = 0, \\ -(1/2)^{1/2}(t_x + it_y), & \mu_\tau = +1. \end{cases} \tag{20}$$

Oscillations with $\tau = 0$ correspond to the oscillation of the isoscalar (total) density. Oscillations with $\tau = 1$, $\mu_\tau = 0$, $I^\pi = 1^-$ correspond to the oscillation of the $\rho_{\tau,\,\mu=1,0}$ component of the isovector density and describe the oscillation of protons and neutrons moving in antiphase (oscillations of neutrons against protons), and deformation leads to splitting of the $E1$ giant resonance (GDR) peak [32]. Oscillations with $\tau = 1$, $\mu_\tau = \pm 1$ describe the β^+/EC (oscillations of proton holes against neutrons) and β^- decays (oscillations of protons

against neutron holes), and the peaks in $S_\beta(E)$ for deformed nuclei should also be split [11, 31]. Splitting of the peak in the strength function (Fig. 13) for the Gamow–Teller β^+/EC decay of the deformed ^{160g}Ho nucleus was experimentally observed, which corresponds to oscillation anisotropy of the isovector density component $\rho_{\tau,\mu=1,1}$. Anisotropy of the spin–isospin density oscillations results in the difference of oscillation energies $\langle E\rangle_\gamma - \langle E\rangle_\beta$ of proton holes against neutron particles perpendicular to the symmetry axis and along the symmetry axis, which is about 1 MeV in the deformed ^{160}Dy nucleus. The isovector density oscillation amplitudes are tensors not only in isospace and orbital space, which leads to splitting of the $E1$ resonance in deformed nuclei, but also in spin space, which leads to splitting of the peaks in $S_\beta(E)$ in deformed nuclei.

For the first-forbidden β^+/EC transitions in the ξ approximation (Coulomb approximation), the important configurations are those of the proton hole–neutron particle type coupled to the moment 0^- or 1^-: $[\nu p \times \pi h]$. The presence or absence of the resonance structure in the strength functions for FF β^- or β^+/EC transitions has been an open question for a long time. In [11–13], it was experimentally established that $S_\beta(E)$ for the first-forbidden β^+/EC decays of ^{160g}Ho (Fig. 14) and isomer ^{160m}Ho (Fig. 15) has a resonance structure. Fine structure of resonance in GT β^+/EC of isomer ^{160m}Ho [11–13] was also observed (Fig. 16).

The resonance nature of $S_\beta(E)$ for GT and FF transitions in spherical, transitional and deformed nuclei was experimentally proved. The fine structure of resonances in $S_\beta(E)$ was measured (Figs. 9–17). Strong configuration mixing at high excitation energies and level densities should result in disappearance of the resonant structure in the strength functions $S_\beta(E)$. The approximate symmetry of nuclear interaction prevents from mixing of

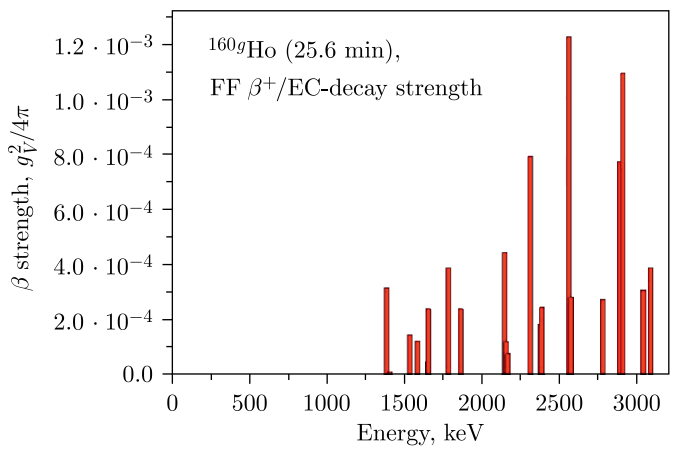

Fig. 14. Fine structure [11–13] of the g.s. FF β^+/EC-decay strength function for deformed nuclei ^{160}Ho

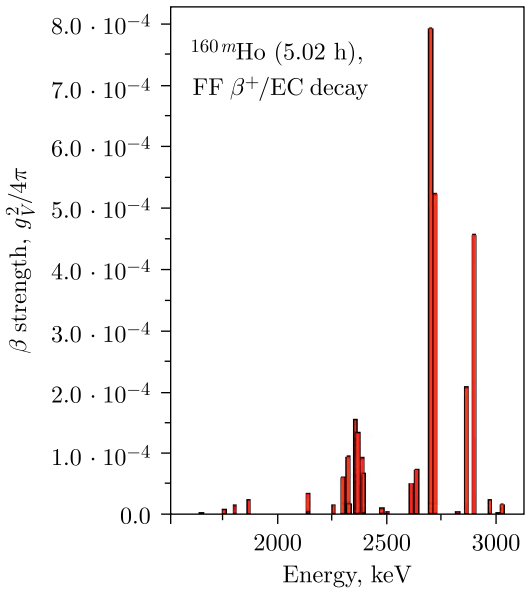

Fig. 15. Fine structure of the isomeric state FF β^+/EC-decay strength function for deformed nuclei ^{160m}Ho [11–13]

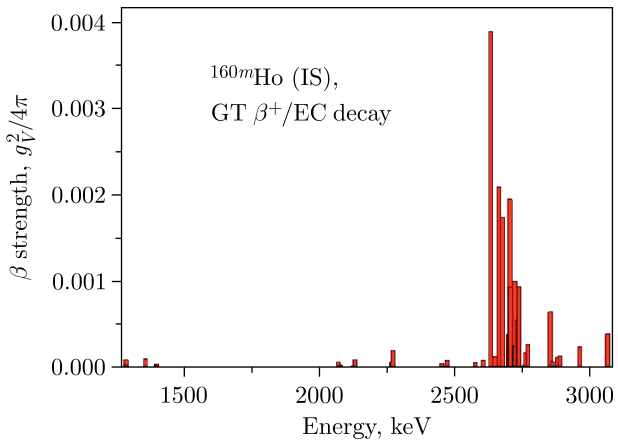

Fig. 16. Fine structure of the isomeric state (IS) GT β^+/EC-decay strength function for deformed nuclei ^{160m}Ho ($T_{1/2} = 5.02$ h, $Q_{\text{EC}} = 3346$ keV) [11–13]

some configurations. For configurations populated by Gamow–Teller β^+/EC transitions, the mixing is weaker because of partial $SU(4)$ spin–isospin symmetry of interaction within the nucleus [4, 6, 11]. For FF β^+/EC transitions, the resonance structure [11–13] was also observed in the strength

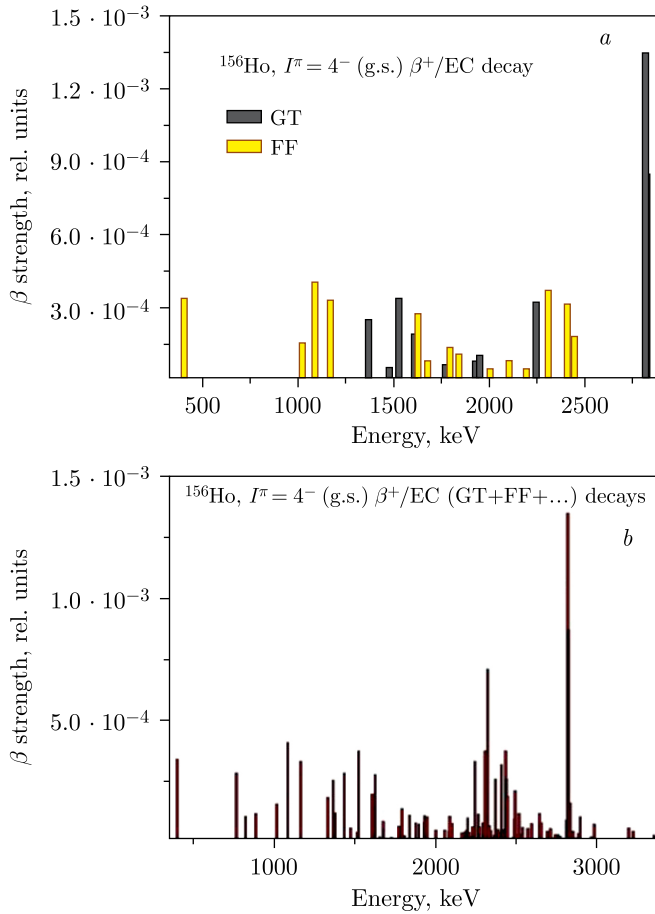

Fig. 17. Structure of the strength function for the GT and FF β^+/EC decay of transitional nuclei ^{156g}Ho ($T_{1/2} = 56$ min, $Q_{EC} = 5.05$ MeV) [30]. *a*) Components of $S_\beta(E)$ for which it was possible to determine the type (GT or FF) of β^+/EC decays; *b*) all observed $S_\beta(E)$ components

function $S_\beta(E)$ (Figs. 14 and 15). The resonance structure of the strength function for first-forbidden β^+/EC transitions may indicate that interaction in the nucleus is characterized by some partial symmetry. This means that configurations populated by FF transitions are also distinguished in approximate quantum numbers among the neighboring levels of the daughter nucleus, and strong configuration mixing does not occur. The type of such symmetry corresponding to the first forbidding is now an open question.

Since there are no sufficient data for finding the fine structure of $S_\beta(E)$ at the ^{156}Dy excitation energies above 3 MeV, Fig. 17 presents $S_\beta(E)$ in relative

units. At the excitation energies of 2.8 MeV, the resonance is observed in $S_\beta(E)$. The total absorption gamma spectrum (TAGS) (Fig. 7) also indicates the presence of a peak in $S_\beta(E)$ in the above-mentioned region of excitation energies. For some energy regions, the intensities of FF β^+/EC transitions are comparable with those for Gamow–Teller transitions (Fig. 17).

4. STRUCTURE OF THE β-DECAY STRENGTH FUNCTIONS AND DELAYED PROCESSES

The previously dominant statistical model [26] assumed that there were no resonances in $S_\beta(E)$ in the Q_β window, and the relations $S_\beta(E) = \text{const}$ or $S_\beta(E) \sim \rho(E)$, where $\rho(E)$ is the level density of the daughter nucleus, were considered to be good approximations for medium and heavy nuclei for excitation energies $E > 2{-}3$ MeV. Ideas about the nonstatistical structure of the strength functions $S_\beta(E)$ have turned out to be important for widely differing areas of nuclear physics including the description of delayed processes by considering the $S_\beta(E)$ structure [1–4]. For correct analysis of the beta-delayed processes probabilities $P_{\beta d}$ (Fig. 18), it is necessary to have information on $S_\beta(E)$ peak positions, intensities, widths, and fine structures [1–6, 11].

The probability of β-delayed processes $P_{\beta d}$ is defined as follows [1–6, 11, 33–42]:

$$P_{\beta df} = \frac{\int\limits_0^{Q_\beta} S_\beta(E)\, f(Q_\beta - E)\Gamma_d(E)/\Gamma_{\text{tot}}(E)\, dE}{\int\limits_0^{Q_\beta} S_\beta(E)\, f(Q_\beta - E)\, dE}, \qquad (21)$$

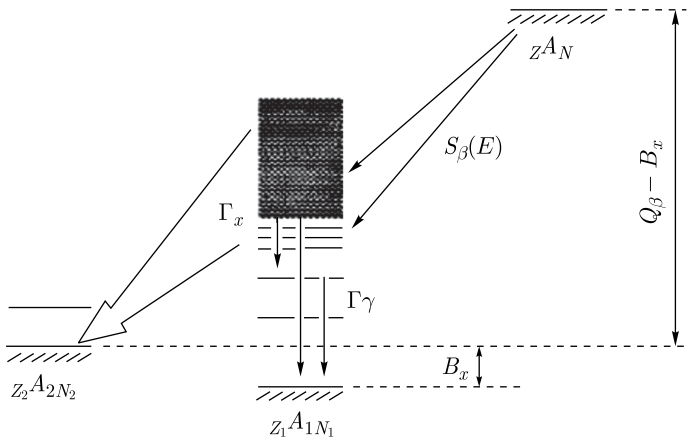

Fig. 18. Energy relationships for emission of delayed particles. B_x is the binding energy of the particle emitted after the β decay, Q_β is the total β-decay energy, Γ_x is the width of the decay channel with emission of a delayed particle

where $\Gamma_d(E)$ is the delayed process width and $\Gamma_{\text{tot}}(E)$ is the total width. Since the energy and relative intensities of peaks in $S_\beta(E)$ should be known for calculation of $P_{\beta d}$, the theory often gives rather correct values for $P_{\beta d}$. However, when only the "tail" of the $S_\beta(E)$ peak falls within the energy-allowed region Q_β, the theoretical calculation yields the correct result only if the fine structure of $S_\beta(E)$ is taken into consideration [1–4]. The most significant region of excitation energies in the daughter nucleus [11] is $\delta = Q_\beta - E_{\text{thr}}$, where $E_{\text{thr}} = E_{\text{II}}$ for delayed fission, E_{II} is the energy of the minimum in the second potential well for the double-humped fission barrier, $E_{\text{thr}} = B_n$ for delayed neutrons, B_n is the neutron binding energy, $E_{\text{thr}} = B_p + E_{po} + q$ for delayed protons, B_p is the proton binding energy, E_{po} is the excitation energy at which the proton emission probability is comparable with the gamma emission probability, and $q \approx 1-2$ MeV. For the probability of delayed fission and delayed proton and alpha particle emission, the structure of $S_\beta(E)$ in the excitation energy region $\delta = Q_\beta - E_{\text{thr}}$ is very significant. For the probability of delayed neutron emission, the integral value of $S_\beta(E)$ in the region $(Q_\beta - E_{\text{thr}})$ is significant:

$$P_{\beta df} = \frac{\int\limits_{E_{\text{thr}}}^{Q_\beta} S_\beta(E)\, f(Q_\beta - E)\Gamma_d(E)/\Gamma_{\text{tot}}(E)\, dE}{\int\limits_{0}^{Q_\beta} S_\beta(E)\, f(Q_\beta - E)\, dE}. \qquad (22)$$

Naturally, for the analysis of delayed particle spectra, the structure of $S_\beta(E)$ is always important. When the peak in $S_\beta(E)$ is near Q_β (Fig. 19, *a*) or E_{thr} (Fig. 19, *b*), the information on the fine structure of $S_\beta(E)$ is very important for correct calculation of $P_{\beta d}$. For the delayed proton and alpha particle emission and delayed fission processes (21), (22), when the energy dependence of the function $\Gamma_d(E)/\Gamma_{\text{tot}}(E)$ is stronger than that of the function

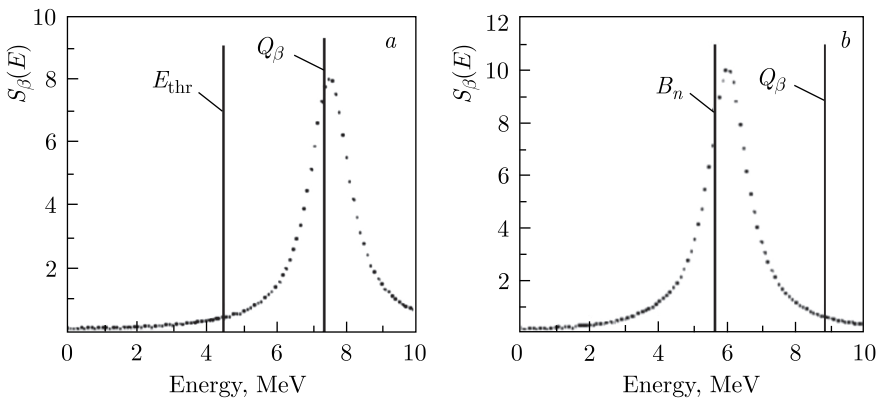

Fig. 19. Different $S_\beta(E)$ peak positions in the $(Q_\beta - E_{\text{thr}})$ energy window. Descriptions for (*a*) and (*b*) are given in the text

$f(Q_\beta - E)$, $P_{\beta d}$ increases when the peak in $S_\beta(E)$ is in the region of the energies Q_{EC} for the β^+/EC decay or Q_β for the β^- decay. In this case, the statistical theory [26], which assumes that $S_\beta(E) \sim \rho(E)$, where $\rho(E)$ is the level density of the daughter nucleus, may accidentally turn out that $P_{\beta d}$ values agree rather well with the experiment (Fig. 19, *a*) both for statistical and nonstatistical theories. Of course, the nonstatistical approaches that take the $S_\beta(E)$ structure into consideration should be used for correct calculation of $P_{\beta d}$. For emission of delayed neutrons at $E > B_n$, the energy dependence of the function $f(Q_\beta - E)$ can be stronger than that of the function $\Gamma_d(E)/\Gamma_{\text{tot}}(E)$ and $P_{\beta d}$ will increase as the $S_\beta(E)$ peak shifts to the energy range $E \sim B_n$ (Fig. 19, *b*). For the GT β^- decay of neutron-rich nuclei, two types of peaks in $S_\beta(E)$ are of major importance. One is associated with configurations like the back-spin flip (BSF, Fig. 2), while the other — with configurations like core polarization (CP, Fig. 2). The CP peak corresponds to the situation shown in Fig. 19, *a*, and the BSF peak — to that in Fig. 19, *b*.

The spectrum of delayed particles depends on the structure of the nuclear states populated in the β decay and the structure of the states populated after the delayed process [1–6, 11, 33–35]. Spectra of delayed particles are governed both by the shape and structure of the β-transition strength function $S_\beta(E)$ and by the probability for emission of delayed particles from the populated states or by the ratio $\Gamma_d(E)/\Gamma_{\text{tot}}(E)$. For example, the GT β^- decay of the ^{135}Sb nucleus populates three-quasiparticle states in the ^{135}Te nucleus. The transition to the ground state of the even–even nucleus ^{134}Te with emission of delayed neutrons from the three-quasiparticle states of the ^{135}Te nucleus is forbidden if the ground state of the ^{134}Te nucleus is treated as a quasiparticle vacuum [4]. At the same time, emission of delayed neutrons with excitation of the 2^+ state in ^{134}Te is allowed because the structures of the ground and excited states are different. This conclusion has been experimentally confirmed: for all states populated in the β^- decay of ^{135}Sb, the neutron decay to the ground state of ^{134}Te is forbidden by a factor of 30–40. Therefore, since the structure of the initial and final states is essential, the statistical methods can be used to calculate the width ratio $\Gamma_d(E)/\Gamma_{\text{tot}}(E)$ only as an approximation [4, 6, 11]. When delayed processes are investigated, the resonance character of $S_\beta(E)$ both for transition of the GT and FF types needs to be considered. Experimental data on the resonance character of $S_\beta(E)$ for FF transitions have been obtained [11–13]. Nevertheless, the effect of the resonance character of $S_\beta(E)$ for FF β transitions on the probability of delayed processes is still poorly investigated.

Delayed fission, i.e., fission of nuclei after the β decay (Fig. 20), is a unique tool for studying fission barriers far from the β-stability line. However, in order to obtain information on the fission barrier, one should know the shape of $S_\beta(E)$ [1–4]. The delayed fission probability (27) and (28) substantially depends on the structure of the strength function for β transitions. The effect of the structure of the β-decay strength function on the probability of delayed fission was investigated for the first time in [1–3]. Then, the method developed

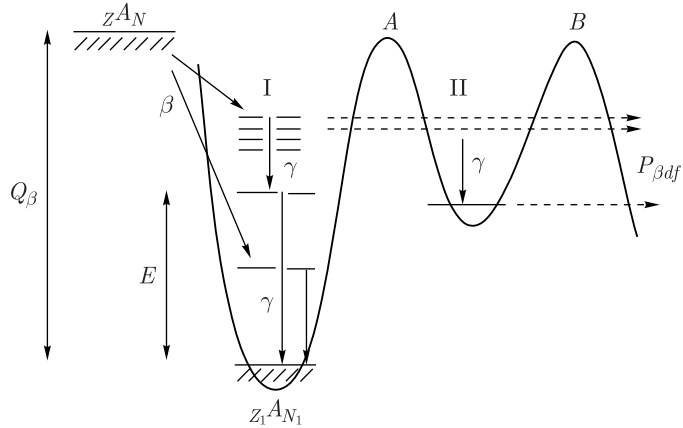

Fig. 20. Scheme of β-delayed fission (βdf). The heights of the inner (A) and outer (B) fission barriers of the daughter nucleus are indicated

for the description of delayed processes by considering the $S_\beta(E)$ structure was used to analyze delayed fission of a wide range of nuclei [1–6, 11, 29].

The delayed-fission probability (Fig. 20) substantially depends on the resonance structure of $S_\beta(E)$ both for β^- and β^+/EC decays. It can therefore be concluded from the analysis of the experimental data on delayed fission that the latter can be correctly described only by using the nonstatistical β-transition strength function reflecting nuclear-structure effects [1–6].

Beta-delayed fission gives a possibility to investigate the fission barrier for nuclei far from the β stability. However, before any information on the fission barrier can be extracted, the effect of low-lying structures in the β-decay strength function $S_\beta(E)$ on the βdf branching ratio has to be considered.

The delayed fission of $^{236,\,238}$U [1, 2, 4, 6, 11] takes place after the β decay of $^{236,\,238}$Pa. Calculation of $S_\beta(E)$ for $^{236,\,238}$Pa was carried out in [1, 2, 4] within the framework of the shell model with residual GT spin–isospin interaction. The majority of the β-transition strength (Fig. 20) is concentrated in the GT giant resonance situated near the isobar-analog state. At the energies of 7–8 MeV below the analog state, a second peak is observed, which is due to transitions of the spin-flip type and core polarization. At the energies of about 18 MeV below the analog state, a peak arises from transitions of the back-spin-flip type (Figs. 2 and 21) which make the major contribution to the probability for the delayed fission of $^{236,\,238}$U.

Table 3 presents the calculated values of $P_{\beta df}$ for various assumptions about $S_\beta(E)$. Calculation of $P_{\beta df}$ using statistical models for $S_\beta(E)$ gives values of $P_{\beta df}$ which are 5–6 orders of magnitude larger than the experimental ones in the case of $S_\beta(E)$ to the level density of daughter nuclei, $S_\beta \sim \rho(E)$, while for $S_\beta = \text{const}$, the $P_{\beta df}$ values are 2–3 orders of magnitude larger for ^{236}U and ^{238}U. Thus, for the delayed fission of ^{236}U and ^{238}U, the assumptions used in statistical models, $S_\beta = \text{const}$ and $S_\beta \sim \rho(E)$, give values of $P_{\beta df}$ which are significantly larger than the experimental values, while the use of

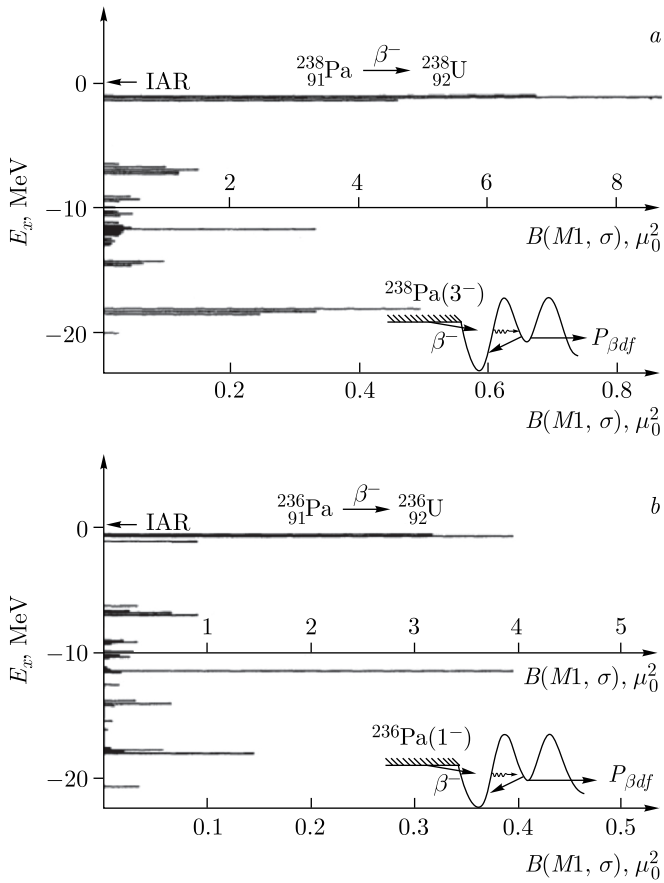

Fig. 21. Strength function $S_\beta(E)$ for the β^- decay of ^{238}Pa (*a*), ^{236}Pa (*b*) and the ^{236,238}U fission barriers. $B(M1,\sigma) = 11\,633/(T \cdot ft) = \text{const} \cdot S_\beta(E)$, where T is the isospin of the ground state of the daughter nucleus, $B(M1,\sigma)$ is in units of μ_0^2 (μ_0 — the nuclear magneton), and ft is in seconds

Table 3. **Delayed-fission probabilities $P_{\beta df}$ for ^{236}U and ^{238}U: experimental values and values calculated with various assumptions about the β-decay strength functions**

Nucleus	Values of $P_{\beta df}$ for various choices of $S_\beta(E)$			Experiment
	$S_\beta(E) = \text{const}$	$S_\beta(E) \sim \rho(E)$	Nonstatistical model, $S_\beta(E)$ from Fig. 21	
^{236}U	$6 \cdot 10^{-7}$	$6 \cdot 10^{-4}$	10^{-12}	10^{-9}
^{238}U	$2 \cdot 10^{-5}$	10^{-2}	10^{-8}	10^{-8}

the nonstatistical $S_\beta(E)$ reflecting nuclear structure effects leads to better agreement between the experimental and calculated values of $P_{\beta df}$ for ^{238}U. The latter calculation predicts that $P_{\beta df}$ decreases in going from ^{238}U to ^{236}U, also in agreement with the data.

The delayed fission $^{256m}\mathrm{Es} \to {}^{256}\mathrm{Fm} \to \beta df$ was studied in [38]. The value of the delayed-fission probability was found to be $P_{\beta df} \approx 2 \cdot 10^{-5}$, and the decay scheme of ^{256}Fm was studied. It was shown experimentally that delayed fission occurs mainly after the β^- decay to the level with excitation energy $E \approx 1425$ keV, i.e., a manifestation of resonance structure in $S_\beta(E)$ in delayed fission was discovered experimentally. The calculations also predict the presence of a resonance in $S_\beta(E)$ near excitation energies $E \approx 1.5$ MeV [6, 11].

A rather large fraction of delayed fission is observed [39] for the β^+/EC delayed fission of ^{232}Pu, $^{232}\mathrm{Am} \to {}^{232}\mathrm{Pu} \to \beta df$: $P_{\beta df} \approx 1.3 \cdot 10^{-2}$. The data on the delayed fission after the β^+/EC decay of ^{232}Am were used in [39] to find the parameters of the inner fission barrier (barrier A in Fig. 20) of ^{232}Pu. The results of [39], obtained by assuming $S_\beta(E) = \mathrm{const}$, give $P_{\beta df} = 1.3 \times$ $\times\, 10^{-2}$ for the height of the inner fission barrier $E_A = 5.3$ MeV, which is 1–2 MeV higher than predicted by the calculations using the Strutinsky method ($E_{\mathrm{thr}} = 3.5$–4.3 MeV [3]). In [39], it was concluded on this basis that the "experimental" and theoretical values of the fission barriers for ^{232}Pu disagree with each other. However, as was shown in [3], the choice $S_\beta = \mathrm{const}$ is not justified and does not reflect the features of the β^+/EC decay in the particular case of the ^{232}Am nucleus. The structure of the strength function $S_\beta(E)$ of the β^+/EC decay of ^{232}Am was calculated in [3] on the basis of the idea of Gamow–Teller charge-exchange excitations and is shown in Fig. 22. Nonstatistical effects leading to the presence of resonance structure in $S_\beta(E)$ significantly change the analysis of the values of $P_{\beta df}$. The value of the total energy of the β^+/EC decay, $Q_\beta = 5.2$ MeV, is marked by the arrow in Fig. 22 and was obtained by using the Garvey–Kelson mass formula. In Fig. 22, the fission barrier of ^{232}Pu, calculated by the method of Strutinsky shell corrections, is also shown. The following parameters of the fission barrier for ^{232}Pu were used in the calculations of $P_{\beta df}$: $E_B = 4.21$ MeV, $\hbar\omega_A = 0.9$ MeV, $\hbar\omega_B = 0.6$ MeV, and the height of the inner barrier E_A was varied. Assuming $S_\beta(E) = \mathrm{const}$ and $P_{\beta df} = 1.3 \cdot 10^{-2}$, it was found that $E_A = 5.3$ MeV, i.e., the same result as in [39], which is 1–2 MeV higher than in the calculations using the Strutinsky method ($E_{\mathrm{thr}} = 3.5$–4.3 MeV). However, if $S_\beta(E)$ calculated in [3, 4, 6, 11] is used and a realistic width is introduced (FWHM = 1 MeV), then without any fit we find that $E_A = 4.0$ MeV corresponds to $P_{\beta df} = 5.0 \cdot 10^{-2}$, in agreement with experiment [39] and with the Strutinsky calculation of the fission barrier. Therefore, on the basis of the analysis of [3, 4, 6, 11] it can be concluded that:

1) if the structure of $S_\beta(E)$ is taken into consideration in a suitable manner, the experimental data on the delayed fission of ^{232}Pu can be explained;

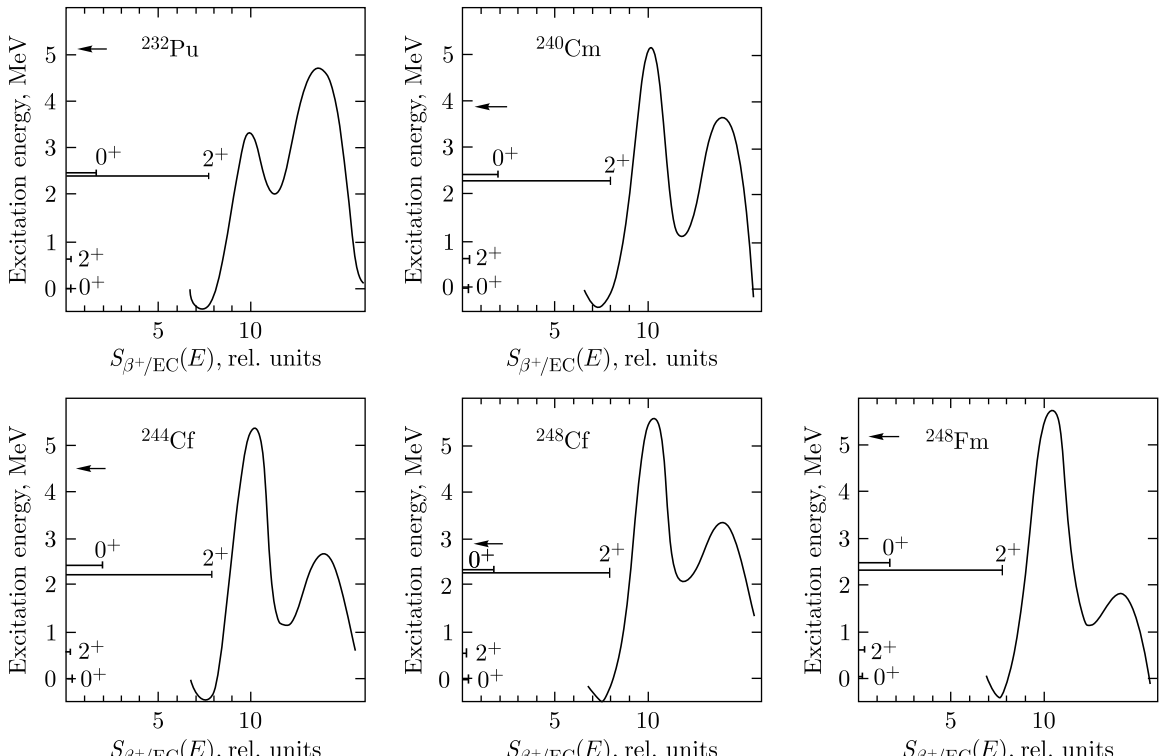

Fig. 22. Structure of the strength functions of the β^+/EC decay of ^{232}Am, ^{240}Bk, ^{244,248}Es, and ^{248}Md (see the text), and fission barriers of ^{232}Pu, ^{240}Cm, ^{244,248}Cf, and ^{248}Fm. The total energies of the EC decay were calculated using the Garvey–Kelson mass formulas and are indicated by the arrows

2) there are no grounds for stating that the fission barriers calculated using the Strutinsky method do not lead to a description of the data on delayed fission, as was done in [39].

In the actinide region, the β^+/EC delayed fission has also been studied for the following processes:

$$^{240}\mathrm{Bk} \rightarrow {}^{240}\mathrm{Cm} \rightarrow \beta df,$$
$$^{244,248}\mathrm{Es} \rightarrow {}^{244,248}\mathrm{Cf} \rightarrow \beta df,$$
$$^{248}\mathrm{Md} \rightarrow {}^{248}\mathrm{Fm} \rightarrow \beta df,$$
$$^{234}\mathrm{Am} \rightarrow {}^{234}\mathrm{Pu} \rightarrow \beta df.$$

In Fig. 22 and Table 4, we give the results of the calculations [3, 4, 6, 11] of $S_\beta(E)$, $P_{\beta df\ \mathrm{theor}}$, and the experimental values of $P_{\beta df\ \mathrm{exp}}$ for a number of nuclei. In the calculation of $P_{\beta df\ \mathrm{theor}}$, the peaks in $S_\beta(E)$ were approximated by Gaussians with FWHM = 1 MeV. The ratio of the "peak" area to the "background" below the peak was chosen to be 100. These parameters for the width and background correspond to the systematics [4, 6, 11]. In this case, the inclusion of the background models the β transitions of various degrees of forbiddenness. We see from Table 4 that the calculated values of $S_\beta(E)$ and $P_{\beta df}$ together with the fission barriers calculated using the Strutinsky method lead to a description of the experiment. Some discrepancies are observed where the experimental values of $P_{\beta df}$ are small (for ^{240}Cm and ^{248}Cf), but by varying the height of the fission barrier within the allowed limits (by no more than 0.5 MeV), agreement with the experiment can be obtained.

The delayed fission of ^{234}Am was studied in [40]. It was shown that $P_{\beta df} = (6.6 \pm 1.8) \cdot 10^{-5}$. Calculations [6, 11] predict that $S_\beta(E)$ has a resonance near the excitation energy $E \approx 2.5$ MeV determining the delayed-fission probability of ^{234}Am. In this case, the experimental value of $P_{\beta df}$ corresponds to a ^{234}Pu fission barrier with the parameters $E_A = 4.7$ MeV, $\hbar\omega_A = 0.9$ MeV, $E_B = 4.2$ MeV, and $\hbar\omega_B = 0.6$ MeV, which agree with the values calculated by the Strutinsky method [6, 11]. It can therefore be concluded from the analysis of the experimental data on delayed fission in the

Table 4. **Experimental [3, 4, 6, 11, 29, 40] and theoretical values of the delayed-fission probabilities $P_{\beta df}$ for ^{232}Pu, ^{244,248}Cf, ^{248}Fm, and ^{240}Cm. The fission barriers were calculated using the Strutinsky method. $P_{\beta df}$ was calculated using the nonstatistical strength functions [3] of the β^+/EC decay (Fig. 22)**

Nucleus	E_A, MeV	E_B, MeV	$\hbar\omega_A$, MeV	$\hbar\omega_B$, MeV	Q_β, MeV	$P_{\beta df\ \mathrm{exp}}$	$P_{\beta df\ \mathrm{theor}}$
^{232}Pu	4.0	4.2	0.9	0.6	5.2	$1.3 \cdot 10^{-2}$	$5 \cdot 10^{-2}$
^{244}Cf	5.3	2.8	0.9	0.6	4.5	$5 \cdot 10^{-4}$	$4 \cdot 10^{-4}$
^{248}Fm	5.7	1.8	0.9	0.6	5.2	$3 \cdot 10^{-3}$	$2 \cdot 10^{-3}$
^{248}Cf	5.7	3.3	0.9	0.6	2.9	$< 10^{-7}$	$2 \cdot 10^{-7}$
^{240}Cm	5.2	3.7	0.9	0.6	3.9	10^{-5}	$9 \cdot 10^{-7}$

actinide region that delayed fission can be correctly described only by using the nonstatistical β-transition strength function reflecting nuclear-structure effects [1–4, 6, 11].

The delayed fission of a number of preactinide nuclei can be used as a test for checking the various models used to calculate $S_\beta(E)$ or the fission barriers. Studies of the β^- delayed fission [6, 11, 42] $^{232}\mathrm{Fr} \rightarrow {}^{232}\mathrm{Ra} \rightarrow \beta df$ are very useful for this. The experimental estimate $P_{\beta df\ \mathrm{exp}} < 2 \cdot 10^{-6}$ for ^{232}Ra was obtained in [43]. The experimental estimate for $P_{\beta df\ \mathrm{exp}}$ strongly contradicts the theoretical value [44] $P_{\beta df\ \mathrm{theor}} \approx 0.3$. The calculations of $P_{\beta df}$ are very sensitive to parameters like the total β-decay energy Q_β, the height of the fission barrier B_f, the barrier curvature $\hbar\omega_f$, and the structure of the β-decay strength function. The dependence of $P_{\beta df}$ on the barrier height and curvature $\hbar\omega_f$ is especially strong in some cases. The calculations performed in [6, 11, 42] showed that for the β^- decay of ^{232}Fr, the strength function $S_\beta(E)$ has a maximum at excitation energy $E^* \approx 5.5$ MeV and can be approximated by a Gaussian of width FWHM $= 1$ MeV. If the parameter of the effective one-hump fission barrier of ^{232}Ra is chosen to be $\hbar\omega_f = 1$ MeV, the experimental estimate $P_{\beta df\,\mathrm{exp}} < 2 \cdot 10^{-6}$ corresponds to the barrier height $B_f > 7.7$ MeV in ^{232}Ra. The value of Q_β was chosen as in [45] (systematics): $Q_\beta = (5.7 \pm 0.7)$ MeV.

Theoretical calculations [46] indicate that the fission barriers for ^{228}Ra and ^{232}Ra are roughly identical. Experimental data on the effective one-hump barrier of ^{228}Ra are given in [47, 48]: $B_f \approx 7.8$ MeV, $\hbar\omega_f = 0.9$ MeV; and $B_f = (8.7 \pm 0.4)$ MeV. Thus, the estimate [42] $B_f > 7.7$ MeV for the barrier in ^{232}Ra is in agreement with a number of experimental and theoretical results. The value of $P_{\beta df}$ obtained in [44] is too large, which may be due to an incorrect choice of the barrier parameters.

For nuclei far from the β-stability line, the calculations of $P_{\beta df}$ can give widely differing results if the energy parameters $[Q_\beta,\ B_f,\ S_\beta(E)]$ are not known accurately enough. The solution of the inverse problem, i.e., estimation of the barrier parameters from the data on delayed fission, can give valuable information [6, 11]. However, in this case, it is necessary to have information about the structure of the β-transition strength function. Since the results on the barrier heights estimation from $P_{\beta df}$ will strongly depend on the position and width of $S_\beta(E)$, much more efforts have to be made to investigate the details of $S_\beta(E)$ both experimentally and theoretically.

Delayed proton spectrum [4, 33, 35] has a typical bell shape with the typical half-width of 2–3 MeV. Therefore, the delayed proton spectrum makes it possible to inspect a rather narrow energy interval in $S_\beta(E)$ and obtain information on the $S_\beta(E)$ structure. If this energy interval does not contain an $S_\beta(E)$ peak, the shape of the delayed proton spectrum agrees fairly well with the statistical model. If an $S_\beta(E)$ peak happens to fall within the energy interval determining the emission of delayed protons, no variations in parameters allow the shape of the delayed proton spectrum to be reproduced for a wide range of nuclei if the $S_\beta(E)$ structure is ignored [4, 6, 11]. The for-

mer case is illustrated by the delayed proton spectrum for ^{69}Se [4, 49]. Here (Fig. 23) the calculation within the statistical model with $S_\beta(E) = \text{const}$ fairly well reproduces the "bell"-shape part of the spectrum. Note that statistical calculations with simulation of various fluctuations can in principle yield "peaks" in the spectra of delayed particles, but they do not allow for the description of regularities in intensities and positions of peaks for different nuclei [4, 6, 11].

The latter case is most clearly exemplified by the delayed proton spectrum for ^{109}Te [4, 50]. Here the spectrum of delayed protons can be described only by considering the $S_\beta(E)$ structure (Fig. 24). An adequate description of the resonance structure in $S_\beta(E)$ makes it possible to explain the expe-

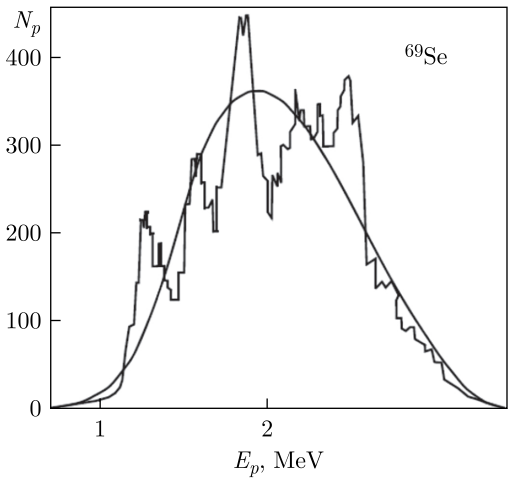

Fig. 23. Spectrum of delayed protons for ^{69}Se [29, 49]. The smooth curve denotes the calculation within the framework of the statistical model with $S_\beta(E) = \text{const}$

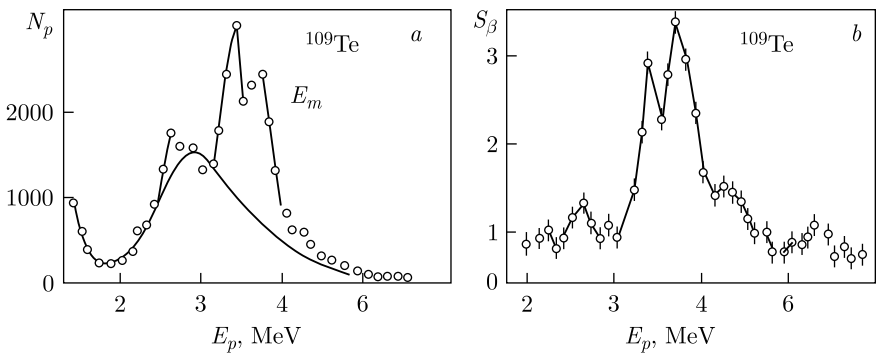

Fig. 24. Spectrum of delayed protons [4, 29, 50] for the ^{109}Te decay (*a*) and $S_\beta(E)$ obtained from it (*b*)

rimental data on the shape of delayed proton spectra for a large variety of nuclei [29, 33, 35].

Below Q_β there are local maxima in $S_\beta(E)$ both for GT and FF β transitions. The fine structures of these maxima in β^+/EC $S_\beta(E)$ are manifested in the form of resonances in the delayed proton spectrum.

The investigation of delayed neutrons (Fig. 25) allows obtaining more detailed information on the $S_\beta(E)$ structure in a wider energy window than the investigation of delayed protons, as there is no Coulomb barrier. Manifestations of the $S_\beta(E)$ resonance structure in spectra of delayed neutrons were observed for many nuclei [4–6, 11, 29, 34]. An example of the strength function for the β^- decay of ^{95}Rb obtained from the analysis of the delayed neutron spectrum [4–6, 51] is shown in Fig. 25 together with the calculations of $S_\beta(E)$ within different models. It is evident from the comparison of the experimental and theoretical data [4–6, 51] that the delayed neutron spectrum for ^{95}Sr can only be correctly described by taking into consideration nonstatistical effects in $S_\beta(E)$.

Some studies quote data only on delayed neutron emission probabilities P_n, i.e., on the probability for emission of a delayed neutron per β^--decay event (22), where $\Gamma_n \equiv \Gamma_d$ and $\Gamma_n/\Gamma_{\text{tot}}$ is the neutron-to-total width ratio for the decay of a level with the excitation energy E. Values for P_n vary between fractions of a percent and tens of percent [4–6, 11, 29, 34] and are sensitive to

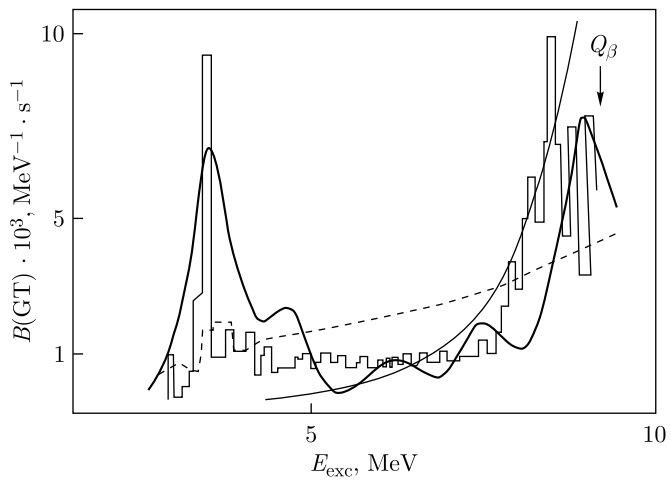

Fig. 25. Strength function for the β^- decay of ^{95}Rb to ^{95}Sr: theoretical calculations using various models and experimental data from analysis of the delayed neutron spectra. The histogram $S_\beta(E)$ is obtained by processing the delayed neutron spectrum of ^{95}Sr, the thin solid line represents the calculation using the statistical model $S_\beta \sim \rho(E)$, the dashed line — the calculation using the gross theory, and the heavy solid line denotes $S_\beta(E)$ calculated using the microscopic model including the Gamow–Teller residual interaction

the shape of $S_\beta(E)$. Only by considering the $S_\beta(E)$ structure, one can describe P_n for a wide range of nuclei [4–6, 11, 52]. However, it is not always possible to obtain close agreement between theoretical and experimental values for P_n and spectral characteristics of delayed neutrons. This is because $S_\beta(E)$ with real peak widths should be used, while reliable calculation of widths is rather problematic. In addition, statistical approaches to calculation of Γ_n and Γ_{tot} are applied, which is a sort of approximation [4, 6, 11].

Another remark, common for calculations of characteristics of delayed processes, is that confidence of the calculations is rather low if the parameters governing delayed process energetics (Q_β, B_x, etc.) are poorly known. This adverse effect on the calculations is especially strong when $S_\beta(E)$ has peaks that are close to Q_β or B_x. Therefore, one should be careful about predictions of characteristics for delayed processes in the region of nuclei far from the β-stability line [4, 6, 11].

For β-delayed fission, β-delayed protons and β-delayed α particles emission probability analysis, the energy dependence of $S_\beta(E)$ is very essential in the $(Q_\beta - E_{\text{thr}})$ window. For β-delayed neutrons, only the total part value of β strength in $(Q_\beta - E_{\text{thr}})$ is generally essential. Of course, for delayed particles spectra analysis, the energy dependence of $S_\beta(E)$ is essential in all cases.

In the β decay, the simple (nonstatistical) configurations are populated and, as a consequence, the nonstatistical effects may be observed in the γ decay of such configurations. In delayed processes analysis, the γ-decay widths Γ_γ are calculated using the statistical model, which, in general, can be just an approximation. As the information about the γ decay is very important for delayed processes analysis, it is necessary to consider the influence of nonstatistical effects on delayed processes probability not only for the β decay, but also for the γ decay. The strong nonstatistical effects were observed both for $M1$ and $E2$ γ transitions in (p, γ) nuclear reactions [6, 53] for the γ decay of nonanalog resonances.

However, since the resonance wave function may also contain an admixture of the statistical component [6, 53], this admixture leads to statistical fluctuations in the distribution of the $E2/M1$ multipole mixture ratio δ values (Fig. 26). From the data on the magnitude of these fluctuations, it is possible to estimate the fraction of the nonstatistical component in the resonance wave function. It turned out that for the considered γ decays of the nonanalog resonances with fixed spin-parity values $I^\pi = 3/2^-$ in ^{59,61,63}Cu, the fraction of the nonstatistical component in the resonance wave function is about several tens of percent (from 20 to 50% [6, 53]).

Experimental data (Figs. 26 and 27) are presented that clearly indicate the manifestation of nonstatistical effects in the γ decay of nonanalog resonances of a compound nucleus in reactions with protons [6, 53]. Nonstatistical effects are associated with elementary modes of nuclear excitations, for example, a proton particle and a neutron hole coupled into spin 1^+, similar as in the GT β decay. At the same time, resonances excited in reactions with neutrons, as a rule, are well described by the statistical model. Such a difference between

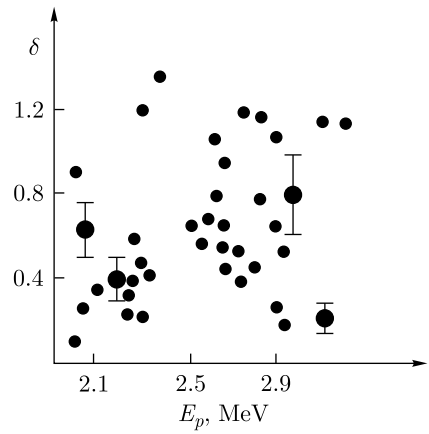

Fig. 26. Experimental dependence of the $E2/M1$ multipole mixture δ for the γ decay of $3/2^-$ nonanalog resonances to the g.s. $(3/2^-)$ of ^{63}Cu. ^{62}Ni $(p,\gamma)^{63}$Cu reaction, $E_p = 1943{-}3175$ keV, $E_{\text{res}} = 8040{-}9250$ keV. The experimental average value of δ is $\langle\delta\rangle = 0.6 \pm 0.1$, while the statistical model gives $\langle\delta\rangle = 0$

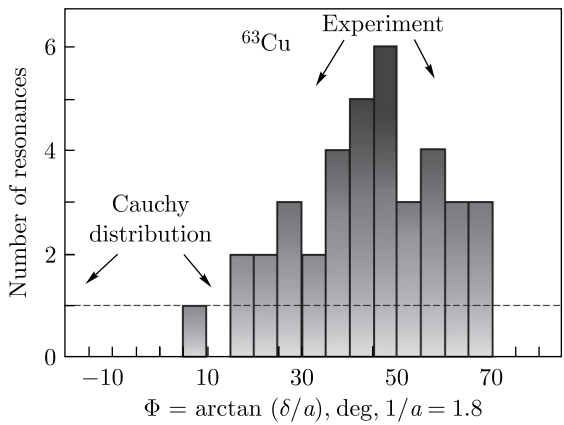

Fig. 27. $E2/M1$ multipole mixture δ for the γ decay of $3/2^-$ nonanalog resonances to the g.s. $(3/2^-)$ of ^{63}Cu. ^{62}Ni $(p,\gamma)^{63}$Cu reaction, $E_p = 1943{-}3175$ keV, $E_{\text{res}} = 8040{-}9250$ keV, and $1/a = \sigma(M1)/\sigma(E2)$, where σ is a standard deviation for $M1$ or $E2$ γ-transition amplitude distributions [53]. Statistical model (Cauchy distribution, dashed line) gives $\langle\delta\rangle = 0$, experiment can be described by the normal distribution with $\langle\delta\rangle = 0.6$. The distribution of experimental values of δ for the reaction ^{62}Ni $(p,\gamma)^{63}$Cu is radically different from the statistical model (Cauchy distribution)

the properties of neutron and proton resonances may be connected with the existence and structure of an excess of neutrons in target nuclei [6, 53].

For correct calculations of the β-delayed processes probabilities $P_{\beta d}$, it is necessary to have information and systematics both on the $S_\beta(E)$ structure and Γ_γ values. Only after proper consideration of nonstatistical effects both for the β decay and γ decay, it is possible to make a quantitative conclusion about delayed processes.

5. SOME FEATURES OF THE β-DECAY STRENGTH FUNCTIONS STRUCTURE IN HALO NUCLEI

Generally, the term "halo" is used when halo nucleon(s) spend(s) at least 50% of the time outside the range of the core potential, i.e., in the classically forbidden region [54–59]. The necessary conditions for the halo formation are the following: small binding energy of the valence particle(s), small relative angular momentum $L = 0, 1$ for two-body or hyper momentum $K = 0, 1$ for three-body halo systems, and not so high-level density (small mixing with nonhalo states). The Coulomb barrier may suppress proton-halo formation for $Z > 10$. Neutron and proton halos have been observed in several nuclei [54–57]. In Borromean systems (Borromean halo), the two-body correlations are too weak to bind any pair of particles, while the three-body correlations are responsible for the system binding as a whole. In states with one and only one bound subsystem, the bound particles moved in phase and were therefore named "tango halo" [16–18, 20].

When the nuclear parent state has the two-neutron Borromean halo structure, the isobar-analog resonance and configuration states can simultaneously have nn, np Borromean halo components in their wave functions [19, 20]. After the $M1$ γ decay of IAR with np Borromean halo structure or the GT β^- decay of parent nuclei with nn Borromean halo structure the states with np halo structure of tango type may be populated [20–22]. When the parent nucleus has nn Borromean halo structure, then after the Gamow–Teller β^- decay of parent state or after the $M1$ γ decay of IAR the states with np tango halo structure or mixed np tango $+ nn$ Borromean halo structure can be populated. Resonances in the GT β-decay strength function $S_\beta(E)$ of halo nuclei may have np tango halo structure or mixed np tango $+ nn$ Borromean halo structure.

Two neutrons that form the nn halo in the ^{6}He ground state occupy the $1p$ orbit ($p_{3/2}$ configuration with a 7% admixture of $p_{1/2}$ configuration). The remaining two neutrons and two protons occupy the $1s$ orbit. The operator $\boldsymbol{T}_-$ lowers the isospin projection by unity without changing the isospin value. Therefore, the action of the operator $\boldsymbol{T}_-$ on the g.s. wave function for the ^{6}He nucleus ($T = 1$, $T_z = 1$) results in the formation of the analog state with the configuration corresponding to the pn halo [60]. This IAR is in the ^{6}Li nucleus ($T = 1$, $T_z = 0$) at the excitation energy of 3.56 MeV. The width of this state is $\Gamma = 8.2$ eV, which corresponds to the half-life $T_{1/2} = 6 \cdot 10^{-17}$ s. The theoretical and experimental data indicate that this IAR state has an np halo [17, 60–62]. Formation of configuration states is prohibited by the Pauli principle. The isobar-analog state (IAS) of the ^{6}He g.s. (nn Borromean halo nucleus), i.e., 3.56 MeV, $I = 0^+$ state of ^{6}Li, has an np halo structure of Borromean type [17, 18, 60].

In the general case [63], IAS (Figs. 28 and 29) is the coherent superposition of the excitations like neutron hole–proton particle coupled to form the momentum $J = 0^+$. The IAS has the isospin $T = T_z + 1 = (N - Z)/2 + 1$, where $T_z = (N - Z)/2$ is the isospin projection. The isospin

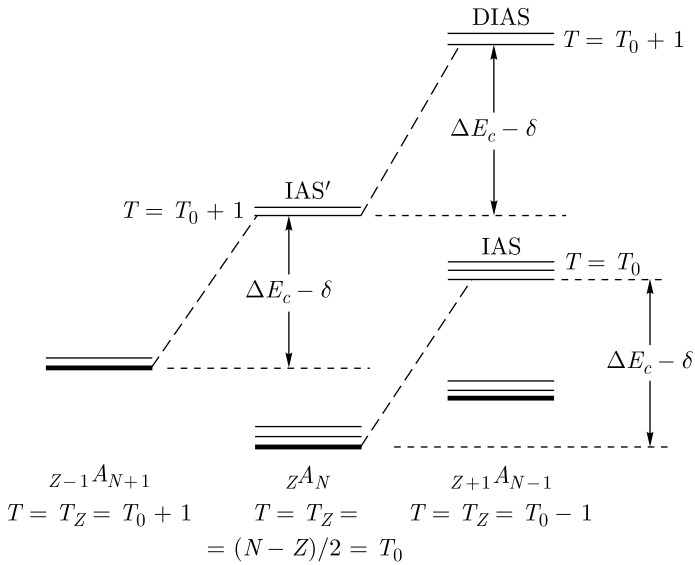

Fig. 28. Diagram of analog (isobar-analog) and double analog (double isobar-analog) states, where ΔE_c is the Coulomb energy of the added proton and δ is the difference of the proton and neutron masses

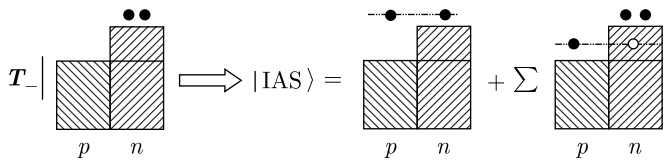

Fig. 29. Structure of the IAS wave function obtained upon the application of the operator $\boldsymbol{T}_-$ to the wave function for the parent nucleus featuring an nn halo [17, 18, 60]. Shaded and open squares stand for the states occupied by protons and neutrons, respectively. Closed circles above the respective squares represent neutrons and protons of the nn and pn halos, while an open circle within the square denotes neutron holes

of the ground state is $T = T_z = (N - Z)/2$. When the IAS energy corresponds to the continuum, IAS can be observed as a resonance. Configuration states (CSs) are not the coherent superposition of such excitations and have $T = T_z = (N - Z)/2$. One of the best studied CSs is the anti-isobar-analog (Fig. 30) state (AIAS). The CS formation may be restricted by the Pauli principle. The double isobar-analog state (DIAS) has the isospin $T = T_z + 2$ and is formed (Figs. 28 and 31) as the coherent superposition of the excitations like two neutron holes–two proton particles coupled to form the momentum $J = 0^+$.

For the Fermi β^- transitions, essential configurations include the states made up of the ground state of parent nucleus by the action of the nucleus

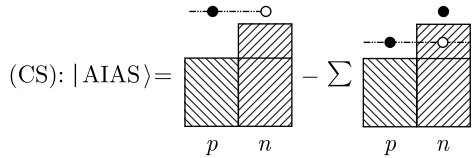

Fig. 30. Structure of the AIAS wave function. In the case where the parent nucleus has an n halo, this structure involves components corresponding to the p and n halos [16–22]. The notation for neutrons, protons, and neutron holes in the anti-analog state is identical to that in Fig. 29

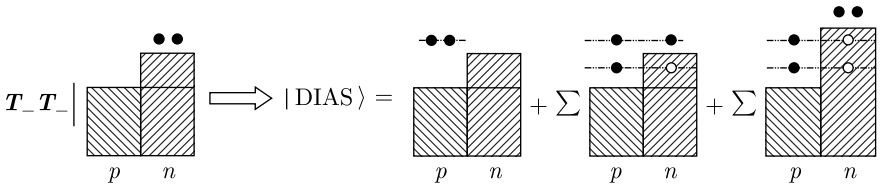

Fig. 31. Structure of the wave function obtained for DIAS with the pp, pn, and nn halos [16–22] upon the application of the operator $\boldsymbol{T}_-\boldsymbol{T}_-$ to the wave function for the parent nucleus possessing an nn halo. The notation for neutrons and protons in the parent nucleus and for neutron holes in the double isobar-analog state is identical to that in Fig. 29

isospin ladder operator $\boldsymbol{T}_-$:

$$\boldsymbol{T}_- = \Sigma\, \boldsymbol{a}_{i+}(\boldsymbol{p}) \cdot \boldsymbol{a}_{i-}(\boldsymbol{n}) = \Sigma\, \boldsymbol{\tau}(\boldsymbol{i})_-. \tag{23}$$

$\boldsymbol{T}_-$ is the operator for transformation of the neutron to the proton without a change in the function of the state in which the particle is. The β-decay strength of the Fermi-type transitions is concentrated in the IAS region. The wave function for IAS and CSs [16–22] involves both components corresponding to the proton–neutron Borromean halo (np halo) and two-neutron Borromean halo (nn halo).

For the GT β^- transitions, essential configurations include the states made up of the ground state of parent nucleus by the action of the Gamow–Teller operator [18, 20–22] $\boldsymbol{Y}_-$:

$$\boldsymbol{Y}_- = \Sigma\, \boldsymbol{\tau}(\boldsymbol{i})_-\, \boldsymbol{\sigma}(\boldsymbol{i}), \tag{24}$$

where $\boldsymbol{\tau}(\boldsymbol{i})_-\, \boldsymbol{\sigma}(\boldsymbol{i})$ is a spin–isospin operator. Acting on the ground state of parent nuclei by the operator $\boldsymbol{Y}_-$ results in formation of configurations of proton particle (πp)–neutron hole (νh) coupled to a spin-parity $I^\pi = 1^+$. These are [4, 6, 11, 20–22] the so-called (Figs. 1–3) core polarization, back spin flip and spin flip configurations.

Coherent superposition [4, 6, 11] of CP, BSF and SF configurations forms the Gamow–Teller resonance. Noncoherent superposition forms resonances in $S_\beta(E)$ at excitation energy E lower than the energy of the GT resonance (so-called satellite or pigmy resonances). Since after action of $\boldsymbol{Y}_-$ operator on nn Borromean halo configuration with $I^\pi = 0^+$ the np tango halo configurations

with $I^\pi = 1^+$ are formed (Figs. 32–34), the GT and pigmy resonances in $S_\beta(E)$ will have components corresponding to np tango halo [20–22]. When neutron excess number is high enough, the SF, CP and BSF configurations may simultaneously have both nn Borromean halo component and np tango halo component and form [16, 20–22] the so-called mixed halo (Figs. 32–34).

Since the operators of the GT β decay and $M1$ γ decay have no spatial components (the radial factor in the $M\lambda\gamma$-transition operator is proportional to $r^{\lambda-1}$), GT β transitions and $M1$ γ transitions between states with similar spatial shapes are favored. When the g.s. does not exhibit halo structure but the excited state may have one, the formation of isomers (halo-isomers) may take place [18].

The IAS in ^{6}Li has the Borromean structure since the n–p subsystem is coupled to the momentum $J = 0^+$, i.e., unbound, whereas the n–p subsystem for the ^{6}Li ground state is coupled to the momentum $J = 1^+$, i.e., bound. According to halo classification, such structure of the ^{6}Li ground state corresponds to the tango halo. As IAS in ^{6}Li has the Borromean structure,

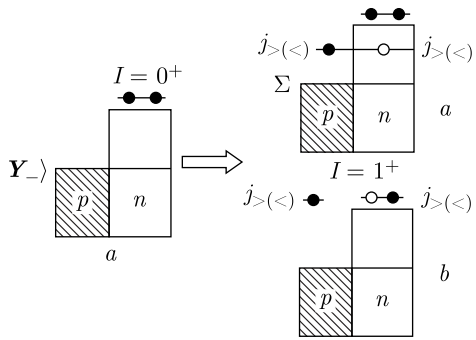

Fig. 32. Proton particle–neutron hole coupled to form the spin-parity $I^\pi = 1^+$ and CP states: *a*) nn Borromean halo component; *b*) np tango halo component

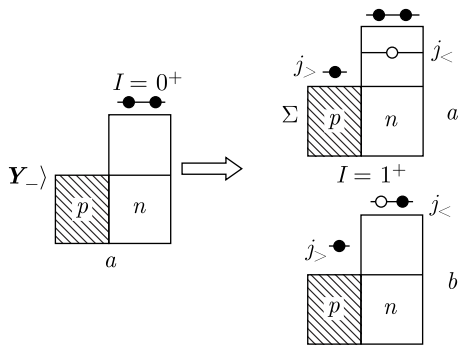

Fig. 33. Proton particle–neutron hole coupled to form the spin-parity $I^\pi = 1^+$ and BSF states: *a*) nn Borromean halo component; *b*) np tango halo component

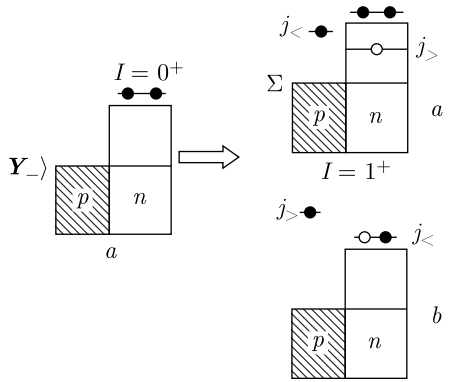

Fig. 34. Proton particle–neutron hole coupled to form the spin-parity $I^\pi = 1^+$ and SF states: *a*) *nn* Borromean halo component; *b*) *np* tango halo component

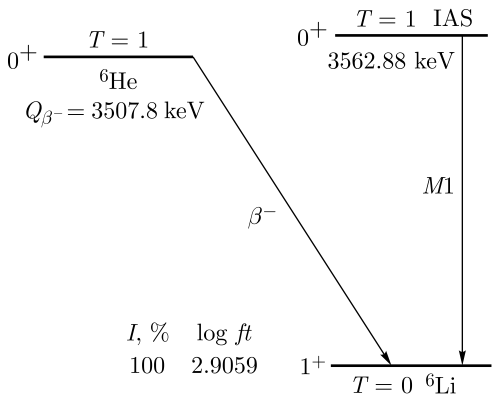

Fig. 35. ^{6}He β decay and $M1$ γ decay of corresponding IAS

the $M1$ γ decay of IAS would be hindered [18, 20–22] if the g.s. of ^{6}Li did not have a halo structure (Fig. 35).

The quantity ft for the Gamow–Teller β decay of the parent nucleus (^{6}He in the ground state) and the reduced probability $B(M1, \sigma)$ for the γ decay of the isobar-analog state (^{6}Li, $E = 3562$ keV) are related by the equation [20–22, 63]

$$ft = 11\,633/[T_0 \cdot B(M1, \sigma)], \tag{25}$$

where T_0 is the isospin of the isobar-analog state, ft is expressed in terms of seconds, and $B(M1, \sigma)$ is expressed in nuclear-magneton $(\mu_0)^2$ units, for $M1$ γ transitions W.u. $= 1.79(\mu_0)^2$. As a result, it turned out that $B(M1, \sigma) = 8.2$ W.u. This means that the $M1$ γ decay of the isobar-analog state in ^{6}Li is enhanced. From experimental value [29], $t_{1/2} = (806.7 \pm 1.5)$ ms, $\log ft = 2.9059$ and using (10)–(13), we determine that

$B(\mathrm{GT}) = (7.63 \pm 0.07) g_V^2/4\pi$ for the GT β^- decay of ^{6}He (Σ (Ikeda sum rule) $= 6(g_{A\mathrm{eff}})^2/4\pi$), i.e., the β^- decay is also strongly enhanced. These experimental facts confirm the hypothesis that the g.s. of ^{6}Li nucleus has a tango halo structure [20–22].

For $|N - Z| \gg 0$ nuclei, the maximum excitation energy corresponds to the main resonance in $S_\beta(E)$ (Figs. 2 and 36). Other, more weak resonances (pygmy resonances), have smaller excitation energies. Such type of $S_\beta(E)$ takes place for ^{11}Be. As GT strength $B(\mathrm{GT})$ for resonance at energy 18.19 MeV ($B(\mathrm{GT}) = 21.8(g_V)^2/4\pi$, Fig. 36) has a large value, we conclude that this resonance ($E_{\mathrm{GTR}} = 18.19$ MeV) in ^{11}Be corresponds to the Gamov–Teller resonance. For ^{11}Be, we have [29] $E_{\mathrm{IAR}} = 21.16$ MeV, i.e., $E_{\mathrm{GTR}} < E_{\mathrm{IAR}}$. Resonances of GT type were not observed in ^{11}Be at the excitation energies more than Q_β. The total strength of all observed β transitions of ^{11}Li is very strong from the point of view of the Ikeda sum rule. For $|N - Z| \gg 0$ nuclei, the theory predicts the maximum excitation energy for the main resonance (GT resonance) [4, 6, 11] in $S_\beta(E)$. If some additional resonance of GT type will exist at excitation energy higher than 18.19 MeV, it will have, since $|N - Z| \gg 0$, comparable strength with the 18.19 MeV resonance. In such situation, we will have additional large GT strength and very strong modification of $g_{A\mathrm{eff}}$ in contradiction with systematic [25]. We neglected possible contribution of the experimentally unobserved GT strength at the energy higher than 18.19 MeV in ^{11}Be to the Ikeda sum rule. Having compared the experimental value [20–22, 29] of total sum of $B(\mathrm{GT})$ with the Ikeda sum rule (10)–(13), we obtained [20–22] that $(g_{A\mathrm{eff}}/g_V)^2 = 1.5 \pm 0.2$ for ^{11}Li.

For $N \approx Z$ nuclei (^{6}Li), the structure of $S_\beta(E)$ may have opposite type, i.e., the minimum [20–22, 64–66] excitation energy corresponds to the main

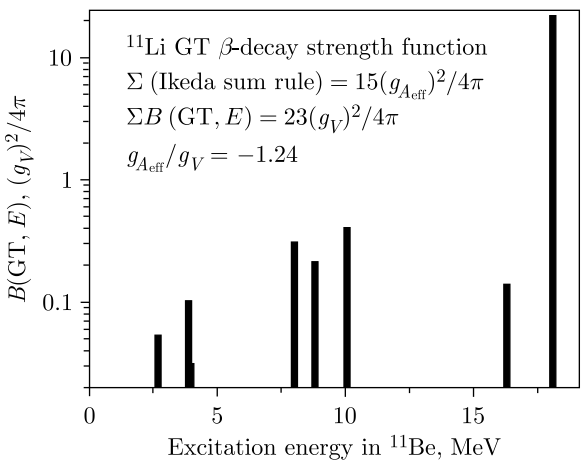

Fig. 36. Structure of the β-decay strength function for ^{11}Li GT β^- decay to ^{11}Be in $(g_V)^2/4\pi$ units [20–22]

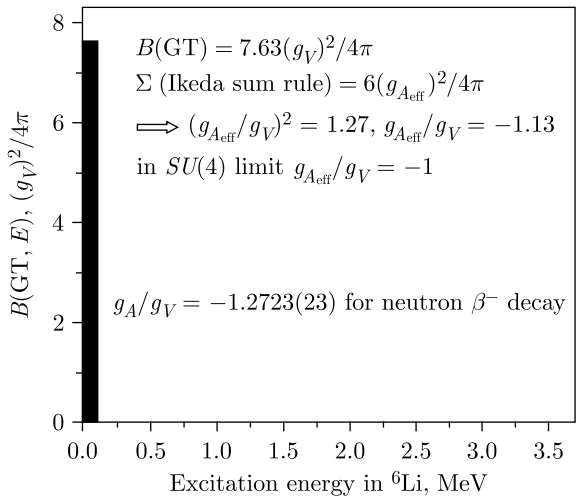

Fig. 37. Structure of the β-decay strength function for ^{6}He GT β^- decay to ^{6}Li in $(g_V)^2/4\pi$ units [20–22]

resonance in $S_\beta(E)$. Such type of $S_\beta(E)$ takes place (Fig. 37) for $^6\mathrm{He} \to {}^6\mathrm{Li}$ β^- decay. Only one additional resonance $I^\pi = 1^+$ with excitation energy 5.65 MeV was observed in ^{6}Li [29]. B(GT) value for this resonance was not measured. Theoretical estimation [24] gives small B(GT) for the 5.65 MeV resonance and we neglected its contribution to the Ikeda sum rule. Having compared the experimental value of $B(\mathrm{GT}) = (7.63 \pm 0.07)\, g_V^2/4\pi$ with the Ikeda sum rule ((10)–(13)) $\Sigma\ B(\mathrm{GT}) = 6(g_{A\mathrm{eff}})^2/4\pi$, we obtained [20–22] that $(g_{A\mathrm{eff}}/g_V)^2 = 1.272 \pm 0.010$ for ^{6}He.

For free-nucleon [25] value $g_{A\mathrm{free}}/g_V = -1.2723(23)$. The renormalization of g_A, which stems from the nuclear-model effects, depends on the nuclear-theory framework chosen to describe the nuclear many-body wave functions involved in the weak processes. This is why the effective values of $g_{A\mathrm{eff}}$ can vary from one nuclear model to another. The origin of the quenching of the g_A value is not completely known [25] and various mechanisms have been proposed for its origin, including tensor effects, the Δ-isobar admixture to the nuclear wave function, relativistic corrections to the Gamow–Teller operator, etc., but a clean separation of these aspects is difficult. Also, the experimental methods of quenching value determination in many cases may have essential uncertainties. One of the model-independent methods for $g_{A\mathrm{eff}}$ determination is the comparison of the experimental total GT β-decay strength with the Ikeda sum rule. For application of this method, it is necessary to have the total GT strength in the energy window allowed for the β decay. Such situation may be realized for the β decay of halo nuclei (^{6}He, ^{11}Li) or for very neutron-rich nuclei where $E_{\mathrm{GTR}} < E_{\mathrm{IAR}}$.

In the case of precise Wigner's spin–isospin $SU(4)$ symmetry, IAR and GTR energies are degenerate and we may expect that $E_{\mathrm{IAR}} \approx E_{\mathrm{GTR}}$.

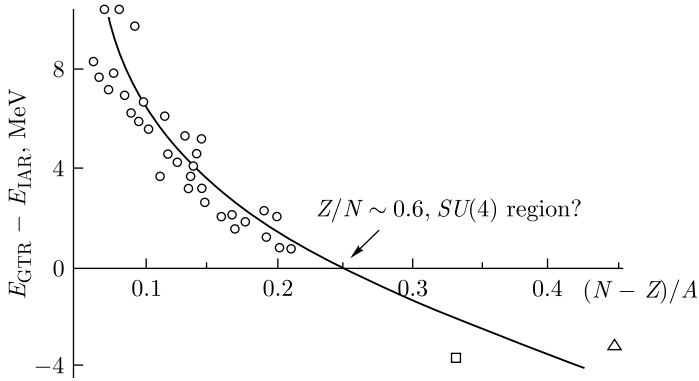

Fig. 38. The difference of the $E_{\mathrm{GTR}} - E_{\mathrm{IAR}}$ energies (circles) as a function of the neutron excess [4, 6, 11, 20–22]. Data for ^{6}He (square) and ^{11}Li (triangle) β^- decays were added [20–22]

In the experimental and theoretical analysis of GTR data, one noticed the tendency of GTR and IAR energies (Fig. 38) to converge with the $(N-Z)/A$ increase [4, 6, 11, 20–22]. This fact may be interpreted as an approximate $SU(4)$ symmetry realization in a definite nuclear area, namely for nuclei with grate $(N-Z)/A$, where spin–isospin $SU(4)$ symmetry determines the nuclear properties ($SU(4)$ region). From simple estimation (Fig. 38), it follows that the value $Z/N \approx 0.6$ corresponds to the $SU(4)$ region [20–22, 67]. The interesting feature shown in Fig. 37 is that the GTR energy is lower than the IAR energy for very neutron-rich nuclei. There is more complicated dependence of $E_{\mathrm{GTR}} - E_{\mathrm{IAR}}$ on $(N-Z)/A$ than linear for the nuclei far from the β-stability line. Shell-model [68, 69] also predicts that the GTR energy can be lower than the IAR energy, i.e., $E_{\mathrm{GTR}} - E_{\mathrm{IAR}} < 0$ for very neutron-rich nuclei. It is thus interesting to measure in more detail the evolution of $E_{\mathrm{GTR}} - E_{\mathrm{IAR}}$ for neutron-rich nuclei far from the β-stability line.

CONCLUSIONS

The current development of experimental technique allows using the methods of high energy resolution nuclear spectroscopy for investigating the fine structure of $S_\beta(E)$. High-resolution nuclear spectroscopy techniques, like the TAGS techniques, provide conclusive evidence for the resonance structure of $S_\beta(E)$ for GT transitions in both spherical and deformed nuclei. With these techniques, it has become possible to experimentally demonstrate the resonance nature of $S_\beta(E)$ for FF transitions and reveal splitting of the peak in the strength function for the GT β^+/EC decay of the deformed nuclei into two components. This splitting indicates anisotropy of oscillation of the isovector density component $\rho_{\tau=1,\,\mu=1}$. The high-resolution nuclear spectroscopy techniques in combination with the TAGS techniques allow incompleteness of nuclear decay schemes to be revealed effectively. They also

allow finding the nuclear excitation energy regions where the intensity of FF β^+/EC transitions is comparable or even higher than that of GT transitions.

After the GT β^- decay of parent state with nn Borromean halo structure or after the $M1$ γ decay of IAR with np Borromean halo structure, the states with np tango halo structure or mixed np tango $+ nn$ Borromean halo structure can be populated. Resonances in the GT β-decay strength function $S_\beta(E)$ of halo nuclei may have np tango halo structure or mixed np tango $+ nn$ Borromean halo structure. Correct interpretation of halo structure is important in experiments on β- and γ-decay study and charge-exchange nuclear reactions analysis. Halo with different structure may be observed for excited states and resonances both in neutron-rich and in proton-rich nuclei. The difference in the halo structure for excited states of nuclei (or excited and ground states) is able to lead to the formation of halo isomers.

Now it seems crucial to develop theoretical models and methods for calculation of $S_\beta(E)$ with deformation of atomic nuclei considered in more detail. To obtain experimental data on the structure of strength functions for both transitions of the GT type and FF transitions in spherical and deformed nuclei is important for further improvement of theoretical approaches to the calculation of $S_\beta(E)$.

The analysis of the complete set of experimental and theoretical results presented in this review unambiguously shows that nonstatistical effects associated with elementary nuclear excitation modes are present in nuclei. Only when nonstatistical effects are taken into consideration, is it possible to correctly describe a large number of processes occurring in nuclei and nuclear reactions. It is expected that nonstatistical effects will be more strongly manifested in nuclei very far from the stability line, especially in the region of Wigner's spin–isospin $SU(4)$ symmetry. It is very attractive to investigate the excitation of the Gamow–Teller resonance and its satellites in heavy-ion reactions. One can therefore hope for qualitatively new facts and ideas about nuclear structure and nuclear reactions, as usually happens when new experimental possibilities are emerging and new phenomena are investigated.

REFERENCES

1. *Izosimov I. N., Naumov Yu. V.* // Bull. Acad. Sci. USSR, Phys. Ser. 1978. V. 42, No. 11. P. 25–32.
2. *Klapdor H. V., Wene C. O., Izosimov I. N., Naumov Yu. V.* // Phys. Lett. B. 1978. V. 78. P. 20.
3. *Klapdor H. V., Wene C. O., Izosimov I. N., Naumov Yu. V.* // Z. Phys. A. 1979. V. 292. P. 249.
4. *Naumov Yu. V., Bykov A. A., Izosimov I. N.* // Sov. J. Part. Nucl. 1983. V. 14, No. 2. P. 175.
5. *Klapdor H. V., Wene C. O.* // J. Phys. G: Nucl. Phys. 1980. V. 6. P. 1061.
6. *Izosimov I. N.* // Phys. Part. Nucl. 1999. V. 30, No. 2. P. 131.
7. *Izosimov I. N., Kalinnikov V. G., Myakushin M. Yu. et al.* // J. Phys. G: Nucl. Part. Phys. 1998. V. 24. P. 831.

8. *Karny M., Nitschke J. M., Archambault L. F. et al.* // Nucl. Instr. Meth. 1997. V. 126. P. 411.
9. *Rubio B., Gelletly W.* // Lect. Notes Phys. / Eds. J. S. Al-Khalili, E. Roeckl. Berlin; Heidelberg: Springer-Verlag, 2009. V. 764. P. 99.
10. *Rubio B., Gelletly W., Naviliat-Cuncic O.* Handbook of Nuclear Physics / Eds. I. Tanihata, H. Toki, K. Toshitaka. Singapore: Springer Nature Pte. Ltd., 2023. P. 349.
11. *Izosimov I. N., Kalinnikov V. G., Solnyshkin A. A.* // Phys. Part. Nucl. 2011. V. 42. P. 963.
12. *Izosimov I. N., Kalinnikov V. G., Solnyshkin A. A.* // J. Phys. Conf. Ser. 2012. V. 381. P. 012054.
13. *Izosimov I. N., Kalinnikov V. G., Solnyshkin A. A.* // Phys. At. Nucl. 2012. V. 75. P. 1324.
14. *Izosimov I. N., Solnyshkin A. A., Khushvactov J.* // JPS Conf. Proc. 2018. V. 23. P. 013004.
15. *Izosimov I. N., Kazimov A. A., Kalinnikov V. G. et al.* // Phys. At. Nucl. 2004. V. 67. P. 1876.
16. *Izosimov I. N.* // Phys. Part. Nucl. Lett. 2018. V. 15. P. 621.
17. *Izosimov I. N.* // Eur. Phys. J. Web Conf. 2016. V. 10. P. 09003.
18. *Izosimov I. N.* // Phys. At. Nucl. 2017. V. 80. P. 867.
19. *Izosimov I. N.* // AIP Conf. Proc. 2015. V. 1681. P. 030006; JINR Preprint E6-2015-41. Dubna, 2015.
20. *Izosimov I. N.* // JPS Conf. Proc. 2018. V. 23. P. 013005.
21. *Izosimov I. N.* // Eur. Phys. J. Web Conf. 2020. V. 239. P. 02003.
22. *Izosimov I. N.* // Phys. Part. Nucl. Lett. 2019. V. 16. P. 754.
23. *Bohr A., Mottelson B. R.* Nuclear Structure. V. 1. New York, Amsterdam: W. A. Benjamin Inc., 1969.
24. *Suhonen J.* From Nucleons to Nucleus. Berlin; Heidelberg: Springer-Verlag, 2007.
25. *Suhonen J.* // Front. Phys. 2017. V. 5. P. 55.
26. *Hansen P. G.* // Adv. Nucl. Phys. 1973. V. 7. P. 159.
27. *Duke C. L., Hansen P. G., Nielsen O. B., Rudstam G.* // Nucl. Phys. A. 1970. V. 151. P. 609.
28. *Alkhazov G. D., Bykov A. A., Vitmann V. D. et al.* // Nucl. Phys. A. 1985. V. 438. P. 482.
29. National Nuclear Data Center, Brookhaven National Laboratory. http://www.nndc.bnl.gov.
30. *Wawryszczuk J., Yuldashev M. B., Gromov K. Ya. et al.* // Z. Phys. A. 1997. V. 357. P. 39.
31. *Izosimov I. N., Solnyshkin A. A., Khushvaktov J. H., Vaganov Yu. A.* // Phys. Part. Nucl. Lett. 2018. V. 15. P. 298.
32. *Bohr A., Mottelson B. R.* Nuclear Structure. V. 2. New York: W. A. Benjamin Inc., 1974.
33. *Borge M. J. G.* // Phys. Scr. 2013. V. 152. P. 014013.
34. *Dimitriou P., Dillmann I., Singh B. et al.* // Nuclear Data Sheets. 2021. V. 173. P. 144.
35. *Blank B., Borge M. J. G.* // Prog. Part. Nucl. Phys. 2008. V. 60. P. 403.
36. *Khuyagbaatar J.* // Eur. Phys. J. A. 2019. V. 55. P. 134.
37. *Andreyev A. N.* // Rev. Mod. Phys. 2013. V. 85. P. 1541.
38. *Hall H. L., Gregorich K. E., Henderson R. A. et al.* // Phys. Rev. C. 1989. V. 39. P. 1866.

39. *Habs D., Kleve-Nebenius H., Metag V. et al.* // Z. Phys. A. 1978. V. 285. P. 53.
40. *Gangrsky Yu. P., Miller M. B., Mikhailov L. V., Kharisov I. F.* // Sov. J. Nucl. Phys. 1980. V. 31. P. 162.
41. *Hall H. L., Gregorich K. E., Henderson R. A. et al.* // Phys. Rev. C. 1990. V. 41. P. 618.
42. *Izosimov I. N.* // Bull. Acad. Sci. USSR, Phys. Ser. 1992. V. 56. P. 39.
43. *Mezilev K. A., Novikov Yu. N., Popov A. V. et al.* // Proc. of the Intern. School–Seminar on Heavy Ion Physics, Dubna, 1990. Dubna: JINR, 1990. P. 199.
44. *Thielemann F.-K., Metzinger J., Klapdor H. V.* // Z. Phys. A. 1983. V. 309. P. 310.
45. *Möller P., Nix J. R.* // At. Data Nucl. Data Tables. 1981. V. 26. P. 165.
46. *Pashkevich V. V.* // Proc. of the Intern. School–Seminar on Heavy Ion Physics, Alushta, USSR, 1983. Dubna: JINR, 1983. P. 405.
47. *Egorov S. A., Rubchenya V. A., Khlebnikov S. V.* // Sov. J. Nucl. Phys. 1987. V. 46. P. 38.
48. *Weber J., Britt H. C., Gavron A. et al.* // Phys. Rev. C. 1976. V. 13. P. 2413.
49. *Hardy C.* CERN Report 76-13. 1976. P. 267.
50. *Bogdanov D. D., Karnaukhov V. A., Petrov L. A.* // Sov. J. Nucl. Phys. 1973. V. 18. P. 1.
51. *Kratz K.-L., Ohm A., Schroder A. et al.* // Proc. of the Intern. Conf. on Nuclei Far from Stability, Helsinger, 1981. P. 317.
52. *Borzov I. N.* // Proc. of 5th Intern. Conf. on Fission and Properties of Neutron Rich Nuclei (ICFN5) / Eds. J. H. Hamilton, A. V. Ramayya. World Scientific Publishing Co. Pte. Ltd., 2014. P. 530.
53. *Izosimov I. N.* JINR Preprint E6-2024-14. Dubna, 2024.
54. *Tanihata I.* // J. Phys. G: Nucl. Part. Phys. 1996. V. 22. P. 157.
55. *Jensen A. S., Riisager K., Fedorov D. V., Garrido E.* // Rev. Mod. Phys. 2004. V. 76. P. 215.
56. *Jonson B.* // Phys. Rep. 2004. V. 389. P. 1.
57. *Tanihata I., Jonson B.* Handbook of Nuclear Physics / Eds. I. Tanihata, H. Toki, K. Toshitaka. Singapore: Springer Nature Pte. Ltd., 2023. P. 986.
58. *Riisager K.* Handbook of Nuclear Physics / Eds. I. Tanihata, H. Toki, K. Toshitaka. Singapore: Springer Nature Pte. Ltd., 2023. P. 1057.
59. *Hammer H.-W.* Handbook of Nuclear Physics / Eds. I. Tanihata, H. Toki, K. Toshitaka. Singapore: Springer Nature Pte. Ltd., 2023. P. 1027.
60. *Suzuki Y., Yabana K.* // Phys. Lett. B. 1991. V. 272. P. 173.
61. *Zhihong L., Weiping L., Xixiang B. et al.* // Phys. Lett. B. 2002. V. 527. P. 50.
62. *Rodkin D. M., Tchuvil'sky Yu. M.* // JETP Lett. 2023. V. 118. P. 153.
63. *Naumov Yu. V., Kraft O. E.* Isospin in Nuclear Physics. Moscow, Leningrad: Nauka, 1972.
64. *Fujita Y., Fujita H., Adachi T. et al.* // Phys. Rev. Lett. 2014. V. 112. P. 112502.
65. *Fujita Y., Fujita H., Adachi T. et al.* // Phys. Rev. C. 2015. V. 91. P. 064316.
66. *Fujita Y., Utsuno Y., Fujita H.* // JPS Conf. Proc. 2018. V. 23. P. 012030.
67. *Izosimov I. N.* // Euras. J. Phys. Funct. Mater. 2019. V. 3. P. 145.
68. *Yoshida S., Utsuno Y., Shimizu N., Otsuka T.* // Phys. Rev. C. 2018. V. 97. P. 054321.
69. *Yoshida S., Utsuno Y., Shimizu N., Otsuka T.* // Phys. Rev. C. 2024. V. 109. P. 029904(E).

Received on October 27, 2025.

Редактор *В. В. Булатова*

Подписано в печать 10.12.2025.
Формат 60 × 90/16. Бумага офсетная. Печать цифровая.
Усл. печ. л. 3,18. Уч.-изд. л. 3,84. Тираж 90 экз. Заказ № 61229.

Издательский отдел Объединенного института ядерных исследований
141980, г. Дубна, Московская обл., ул. Жолио-Кюри, 6.
E-mail: publish@jinr.ru
www.jinr.ru/publish/